SLAC–308
UC–34D
(T)

TOPONIUM—Z^0 INTERFERENCE AND PHENOMENOLOGY OF AN EXTRA Z^0 IN e^+e^- COLLISIONS*

PAULA JEANNETTE FRANZINI

Stanford Linear Accelerator Center
Stanford University
Stanford, California 94305

January 1987

Prepared for the Department of Energy
under contract number DE-AC03-76SF00515

Printed in the United States of America. Available from the National Technical Information Service, U.S. Department of Commerce, 5285 Port Royal Road, Springfield, Virginia 22161. Price: Printed Copy A04, Microfiche A01.

* Ph.D. Thesis.

ACKNOWLEDGMENTS

I would like to thank the members of my committee, Savas Dimopoulos, Michael Peskin, and especially my advisor, Fred Gilman, for their patient guidance and encouragement in teaching me physics, as well as their friendship.

My debts, both physicswise and personally, are to too many people to enumerate here. I am grateful to the members of the SLAC and Stanford theory groups for many enlightening discussions on physics and most other topics, and for providing a warm "home," and to certain of my fellow graduate students for a (sometimes bizarre) sense of humor that kept life from getting boring. I would particularly like to thank my closest friends, Paul Griffin, John and Linda Yeager, Peter Arnold, and most of all Guy Blaylock, for always being there for me. I am indebted to Donald Knuth for making the writing of this thesis much less painful than it could have been.

Finally, this thesis is dedicated to my parents and Bharat Ratra, without whose support and encouragement this might well never have been.

Table of Contents

List of Tables

page

List of Illustrations

page

page

INTRODUCTION

The $SU(3)_c \times SU(2)_L \times U(1)_{em}$ standard model of strong, weak and electromagnetic interactions has been very successful; among the recent demonstrations of its validity have been the discoveries of the $W^{\pm}$ and Z^0 gauge bosons. It would be premature at this point to claim the t quark as discovered; however we are confident of its existence, for example from the absence of flavor-changing neutral currents in B decay. If the mass of the Z^0 is near twice that of the top quark, the toponium bound state will be partially degenerate with the Z^0. Part I of this thesis describes the phenomenology of this situation.

The Higgs sector remains one of the most elusive (and perhaps unsatisfactory) feature of the standard model. It has often been suggested that it should be enlarged, or perhaps replaced altogether by bound states, dynamically generated by a new strong interaction. Even if we stay within "conventional" Higgs structures, there is no reason not to consider multiple Higgs doublets; many currently interesting theories, such as SUSY, left-right symmetric models, and superstring theories, require more than one doublet. Moreover, extra doublets can decouple the CP violation parameters ϵ and ϵ', which could prove useful if, with future measurements, the standard model is unable to account simultaneously for both values. We conclude Part I of this thesis by discussing some limits on such models with extra doublets, and their possible effects on the toponium–Z^0 mixing.

Although experimentally successful, the standard model is not a fundamental theory; it has too many parameters and does not unify the gauge symmetries of nature. A recurring feature of attempted improvements involves embedding it in a larger symmetry group that is exact at higher energies. Many such theories,

in particular grand unified theories and superstring theories, introduce new $U(1)$ gauge symmetries that might remain unbroken to rather "low" energies. These extensions therefore have extra flavor diagonal Z bosons, possibly with masses as low as 120 GeV. In the second part of this thesis we discuss some constraints on these models from low energy phenomenology at e^+e^- colliders.

PART I

TOPONIUM-Z^0 INTERFERENCE*

1. Introduction

The possibility of toponium-Z^0 interference has already been discussed in a number of papers.[1-4] Much of this work, guided by theoretical speculation on the top quark mass, m_t, was concerned with the situation where the Z mass was much higher than $2m_t$. However the discovery of the Z^0 at CERN,[5] and the more recent evidence[6] for a top quark with a mass between 30 GeV and 50 GeV suggests that the scenario where there is a near degeneracy in mass between toponium states and the Z merits a closer and more careful look.[7]

In the next chapter we first present a qualitative discussion of the mixing. We study the mixing of one vector ($J^{PC} = 1^{--}$) toponium state, V, with the Z, solving the problem analytically and studying various limiting cases. There is an exact zero in the amplitude for $e^+e^- \to f\bar{f}$ at the bare (unmixed) mass of the V when the couplings of the bare V state to both e^+e^- and $f\bar{f}$ are zero. We set out the formulas for the couplings, cross sections, asymmetries, etc., and then consider the corrections of allowing non-zero couplings and of including $e^+e^- \to \gamma \to f\bar{f}$. For $\sigma(e^+e^- \to f\bar{f})$ these have a small effect on the overall shape, which still has a strong minimum, whose position is slightly shifted. For the polarization and front-back asymmetries the effects are much more dramatic. The section concludes with the formalism needed for mixing the Z with an arbitrary number

---

* This work has previously been discussed in P. J. Franzini and F. J. Gilman, Phys. Rev. **D32**, 237 (1985) and G. G. Athanasiu, Franzini and Gilman, Phys. Rev. **D32**, 3010 (1985).

of vector toponium states, both below and above the open top threshold, where the off-diagonal mass mixing element becomes complex.

In chapter 3 we briefly discuss heavy quark potentials and the spectrum of toponium states which results. We use Richardson's[8] potential and find roughly 13 states below the open top threshold. Chapter 4 then contains the results following from applying the mixing formalism in Chapter 2 to the Z and the set of toponium states described in Chapter 3. We consider $\sigma(e^+e^- \to f\bar{f})$ in situations where $2m_t$ is less than, roughly equal to, and greater than M_z. There are striking interference patterns observed in $\sigma(e^+e^- \to f\bar{f})$ as well as in the longitudinal and front-back asymmetries. We conclude this chapter with a sobering look at what the experimentally unavoidable spread in beam energies does to these interference patterns. In Chapter 5 we discuss the phenomenology of two-Higgs models, and the bounds imposed on them by their effects on neutral B meson mixing. We then explore what effects an extra Higgs doublet may have on toponium-Z^0 interference.

2. Formalism of mixing

We shall first consider the simplified case of only two states, the Z and one vector ($J^{PC} = 1^{--}$) toponium resonance, V. We begin with a qualitative argument to show that the interference is indeed destructive. To be specific we consider the process $e^+e^- \to \mu^+\mu^-$. This process occurs predominantly as $e^+e^- \to Z_0 \to \mu^+\mu^-$, while another contribution is $e^+e^- \to Z_0 \to V_0 \to Z_0 \to \mu^+\mu^-$ (for now, we neglect the small contributions due to γ couplings). The first term has an amplitude proportional to the propagator

$$\begin{aligned} P_1 &= \frac{1}{(s - M_{Z_0}^2 + i\Gamma_{Z_0} M_{Z_0})} \\ &= \frac{1}{i\Gamma_{Z_0} M_{Z_0}} \end{aligned} \tag{2.1}$$

on the peak of the Z_0 resonance. If, for simplicity, we choose the Z_0 and V_0 resonances to be degenerate, the amplitude from the second contribution is similarly proportional to

$$P_2 = \frac{1}{(i\Gamma_{Z_0} i\Gamma_{V_0} i\Gamma_{Z_0})}. \tag{2.2}$$

Thus we have a relative minus sign between these two amplitudes, i.e., destructive interference.

We can extend this argument by replacing the Z_0 propagator by the iterated series

where the solid line denotes the Z_0 and the double line the V_0. Using a phe-

nomenological $Z_0 - V_0$ coupling a, we get the amplitude to be proportional to

$$\frac{1}{s-M_{Z_0}^2}+\frac{1}{s-M_{Z_0}^2}\cdot\left(a\cdot\frac{1}{s-M_{V_0}^2}\cdot a\cdot\frac{1}{s-M_{Z_0}^2}\right) \tag{2.3}$$

$$+\frac{1}{s-M_{Z_0}^2}\cdot\left(a\cdot\frac{1}{s-M_{V_0}^2}\cdot a\cdot\frac{1}{s-M_{Z_0}^2}\right)^2+\cdots=\frac{s-M_{V_0}^2}{(s-M_{Z_0}^2)(s-M_{V_0}^2)-a^2}\,.$$

(Here, and often in what follows, we will use $M_{Z_0}^2$ to represent the full expression $M_{Z_0}^2 - i\Gamma_{Z_0}M_{Z_0}$.) For energies a few GeV away from a V_0 resonance, $(s-M_{Z_0}^2)(s-M_{V_0}^2)$ is large compared to a^2; as expected, we recover the Z_0 propagator. On the V_0 resonance we get zero for the amplitude—thus we have complete destructive interference.

The amplitude exactly vanishes only if we make some simplifying assumptions:

(1) We have ignored the virtual photon contribution to the process $e^+e^- \rightarrow \mu^+\mu^-$. This is a good approximation, since the photon, by definition, contributes an R-value of about* one, while the R-value on the Z_0 peak is 200. (Note that on the Z_0 peak, the Z amplitude is imaginary while that of the photon is real, so that there is no $\gamma - Z$ interference. However, in general we must compute $Z\gamma V$ mixing. The effect of the photon is small enough to be negligible, except in the determination of the asymmetry parameters.)

(2) We have also implicitly assumed that the width of the V_0 is zero. The expression $s-M_{V_0}^2$ really represents $s-M_{V_0}^2+iM_{V_0}^2\Gamma_{V_0}$ which can only be zero (for a physically allowed value of s) if $\Gamma_{V_0} = 0$. This is also a good approximation,

* The contribution is not exactly one, because R-value is given by the actual photon cross-section divided by the QED point cross-section with α defined at the electron mass scale.

since the expected width of a $t\bar{t}$ $1S$ state (using the Richardson potential) is about 100 keV, compared to Γ_Z=2.7 GeV.

(3) Finally, we have ignored the "direct" couplings of the V_0, that is, the V_0 coupling to fermions through the photon instead of through the Z_0. This approximation is analogous to, and comparable in magnitude with, the second one.

Now let us take a more formal approach. As we are considering mixing between states in a limited energy range far from threshold we may safely use the mass-mixing formalism.[9,10] The 2×2 mass matrix has the form:

$$\mathcal{M}_0^2 = \begin{pmatrix} M_{V_0}^2 - i\Gamma_{V_0}M_{V_0} & \delta m^2 \\ \delta m^2 & M_{Z_0}^2 - i\Gamma_{Z_0}M_{Z_0} \end{pmatrix}, \tag{2.4}$$

and the matrix propagator,

$$\mathcal{D}(s) = \frac{1}{\mathcal{M}_0^2 - s\mathbf{1}}. \tag{2.5}$$

Here $\mathcal{M}_0^2$ is the (undiagonalized) mass matrix with elements expressed in terms of "bare" masses (M_{Z_0} and M_{V_0}) and widths (Γ_{Z_0} and Γ_{V_0}). Within the spirit of the mass-mixing formalism we take the initial widths to be constants, with no explicit functional dependence on mass.[9] Inclusion of such a mass dependence, or working with the mass rather than mass-squared matrix, results in amplitude changes of a few percent in the limited mass range within which we are working. (In the case of mixing between the Z and a new Z' boson, which we consider in the second part of this thesis, the mass dependence of widths will become important, as the Z' may be far away from the Z.)

The off diagonal term δm^2, which induces the mixing, originates in the (vector) coupling of the Z to the t quark contained in the toponium bound state (see Fig. 1). Its value is

$$\begin{aligned} \delta m^2 &= 2\sqrt{3}\,|\psi(0)|\sqrt{M_{V_0}}g_{v,t} \\ &= 2\sqrt{3}\,|\psi(0)|\sqrt{M_{V_0}}\left[\frac{e(1-\frac{8}{3}\sin^2\theta_W)}{4\sin\theta_W\cos\theta_W}\right], \end{aligned} \tag{2.6}$$

where $\psi(0)$ is the wavefunction of the $t\bar{t}$ bound state at the origin and θ_W is the weak mixing angle (so that[11] $\sin^2\theta_W \approx 0.22$). The factor of $\sqrt{3}$ arises from color. For the P states δm^2 is proportional to the derivative of the wave function at the origin, with concomitant much smaller mixing (by roughly an order of magnitude for toponium). This is examined in detail in Ref. 7.

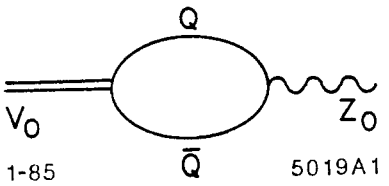

Figure 1. Feynman diagram of the process causing Z_0—V_0 mixing.

For purposes of calculation one can work with the mass matrix in this non-diagonal basis, sandwiching the propagator in Eq. (2.5) between initial and final spinors which express the coupling strength of the "bare" V_0 and Z_0 to the initial

and final states respectively. If we set $g_{V_0} = 0$, $\Gamma_{V_0} = 0$, and $s = M_{V_0}^2$, we have the amplitude

$$\begin{aligned} \mathcal{A} &= \begin{pmatrix} g_Z & g_V \end{pmatrix}_I \left[s - \begin{pmatrix} M_Z^2 - iM_Z\Gamma_Z & 0 \\ 0 & M_V^2 - iM_V\Gamma_V \end{pmatrix} \right]^{-1} \begin{pmatrix} g_Z \\ g_V \end{pmatrix}_F \\ &= \begin{pmatrix} g_{Z_0} & 0 \end{pmatrix}_I \begin{pmatrix} 0 & -\delta m^2 \\ -\delta m^2 & M_{V_0}^2 - M_{Z_0}^2 \end{pmatrix} \begin{pmatrix} g_{Z_0} \\ 0 \end{pmatrix}_F = 0 \end{aligned} \tag{2.7}$$

So in this formalism also, it is easy to see the complete destructive interference. For some purposes, however, it is more useful to go to the diagonal basis, obtaining along the way the physical states and eigenvalues. For this purpose we rewrite Eq. (2.4) as

$$\mathcal{M}_0^2 = \frac{1}{2}(M_{V_0}^2 - iM_{V_0}\Gamma_{V_0} + M_{Z_0}^2 - iM_{Z_0}\Gamma_{Z_0})\mathbf{1} + \Delta^2 \hat{n} \cdot \vec{\sigma} \tag{2.8}$$

where

$$\Delta^2 = \sqrt{(M_{V_0}^2 - iM_{V_0}\Gamma_{V_0} - M_{Z_0}^2 + iM_{Z_0}\Gamma_{Z_0})^2/4 + (\delta m^2)^2}, \tag{2.9a}$$

$$\hat{n} = \cos\theta \hat{z} + \sin\theta \hat{x} \tag{2.9b}$$

and the complex angle θ is given by

$$\sin\theta = \delta m^2/\Delta^2. \tag{2.9c}$$

It is then easy to see that $\mathcal{R}\mathcal{M}_0^2\mathcal{R}^{-1}$, where $\mathcal{R} = e^{\frac{i\theta}{2}\sigma_y}$, is diagonal, with eigenvalues

$$M_V^2 - iM_V\Gamma_V = \frac{1}{2}(M_{V_0}^2 - i\Gamma_{V_0}M_{V_0} + M_{Z_0}^2 - i\Gamma_{Z_0}M_{Z_0}) + \Delta^2 \tag{2.10a}$$

$$M_Z^2 - iM_Z\Gamma_Z = \frac{1}{2}(M_{V_0}^2 - i\Gamma_{V_0}M_{V_0} + M_{Z_0}^2 - i\Gamma_{Z_0}M_{Z_0}) - \Delta^2 \qquad (2.10b)$$

and that the physical eigenstates are

$$|V\rangle = e^{-i\frac{\theta}{2}\sigma_y}\begin{pmatrix}1\\0\end{pmatrix} = \cos\frac{\theta}{2}|V_0\rangle - \sin\frac{\theta}{2}|Z_0\rangle$$

$$|Z\rangle = e^{-i\frac{\theta}{2}\sigma_y}\begin{pmatrix}0\\1\end{pmatrix} = \sin\frac{\theta}{2}|V_0\rangle + \cos\frac{\theta}{2}|Z_0\rangle\,. \qquad (2.11)$$

Since θ is generally complex, R is symmetric but not unitary.

When the narrow state V is far from the Z, these results simplify, and the mixing is characterized by

$$\frac{1}{2}\sin\theta \approx \frac{\theta}{2} \approx \frac{\delta m^2}{M_{V_0}^2 - M_{Z_0}^2 + iM_{Z_0}\Gamma_{Z_0}}. \qquad (2.12)$$

As the magnitude of the right hand side turns out to be (see below) $\lesssim 0.1$ even when $M_{V_0} = M_{Z_0}$, this is even a good approximation when the V and Z are close. The small admixture of the V_0 in the Z has a totally negligible effect, while the corresponding small Z_0 admixture to the V has relatively large effects because of the much larger Z_0 couplings to fermion-antifermion pairs. Alternatively, when the mixing is small, the problem of V decays involving the Z can be treated directly by explicitly calculating diagrams involving an intermediate Z, with identical results[2] to those obtained using Eq. (2.12).

Now let us consider the situation of interest to us when the state V_0 is near the Z_0 and most of the width of the V comes, as we shall see, from mixing with the Z. It is useful to consider then the idealized case where the unmixed state V_0

has no coupling to particular initial and final states, *e.g.*, e^+e^- and $\mu^+\mu^-$. From Eq. (2.11) we see that in this case the couplings of the physical V and Z to the initial and final states are

$$g_V = -\sin\frac{\theta}{2} g_{Z_0}$$

$$g_Z = \cos\frac{\theta}{2} g_{Z_0}. \tag{2.13}$$

Consequently the scattering amplitude

$$A_{fi}(s) = \frac{g_{Vf}g_{Vi}}{M_V^2 - iM_V\Gamma_V - s} + \frac{g_{Zf}g_{Zi}}{M_Z^2 - iM_Z\Gamma_Z - s} \tag{2.14}$$

simplifies to

$$A_{fi}(s) = g_{Z_0 f}g_{Z_0 i}\left[\frac{\sin^2\frac{\theta}{2}}{M_V^2 - iM_V\Gamma_V - s} + \frac{\cos^2\frac{\theta}{2}}{M_Z^2 - iM_Z\Gamma_Z - s}\right] \tag{2.15}$$

At the point $s = M_{V_0}^2 - iM_{V_0}\Gamma_{V_0}$, the (complex) mass squared of the unmixed toponium state,

$$A_{fi}(M_{V_0}^2 - iM_{V_0}\Gamma_{V_0}) = g_{Z_0 f}g_{Z_0 i}\left[\frac{\sin^2\frac{\theta}{2}}{\Delta^2(\cos\theta - 1)} + \frac{\cos^2\frac{\theta}{2}}{\Delta^2(\cos\theta + 1)}\right] = 0 \tag{2.16}$$

when we use the relationship in Eqs. (2.6a,b) between the "dressed" masses and "bare" masses together with the definition of θ in Eq. (2.5c). Therefore there is an exact zero of the amplitude $A_{fi}(s)$ at the position of the unmixed V_0 mass when the unmixed state does not couple to either the initial or final state.

How close is the actual situation to this idealized one? Let us put in some numerical values and insert couplings from the standard model. From the Richardson potential discussed in the next section we take $|\psi(0)|^2 \approx 65$ GeV^3 for the 1S

vector meson ground state of toponium when the top quark mass is such that its mass $M_{V_0} \approx M_Z$ (which we take as[11,12] 93 GeV). According to Eq.(2.6), we then have

$$\delta m^2 = 20 \text{ GeV}^2 \tag{2.17}$$

for mixing of the 1S state with the Z_0.

Preservation of the trace of the mass matrix under diagonalization implies that $M_V^2 - M_{V_0}^2 = -(M_Z^2 - M_{Z_0}^2)$, so the squared masses are shifted equally and oppositely, and similarly for widths. We solve Eqs. (2.10) for the "dressed" masses and widths as a function of M_{V_0}, taking M_{Z_0}=93 GeV and Γ_{Z_0}=2.7 GeV (as we mentioned, $\Gamma_{V_0} = \mathcal{O}(100 \text{ KeV})$[13] and can be neglected at this stage of the calculation), with the results shown in Figs. 2 and 3. Figure 2 shows the shift in the Z mass due to mixing as a function of the mass difference of the bare states (M_{Z_0} is held fixed at 93 GeV, while M_{V_0} is varied). Fig. 3 shows the shift in the toponium width. The mass shift, at most about 4 MeV (i.e. $\Delta M/M \lesssim 5 \times 10^{-5}$), is negligible. On the other hand V does acquire a sizable width which is maximal when the V_0 and Z_0 coincide, at which point

$$\Gamma_V \approx \frac{(\delta m^2)^2}{M_{Z_0}^2 \Gamma_{Z_0}} \approx 18 \text{ MeV}, \tag{2.18}$$

i.e., more than two orders of magnitude greater than the bare width.

The calculation of the cross section, as well as the polarization and front-back asymmetries, is expedited by considering Feynman amplitudes A_{fi} for initial and final fermions of definite handedness, which are in principle separately measurable and hence do not interfere (since the interactions are mixtures of V and A

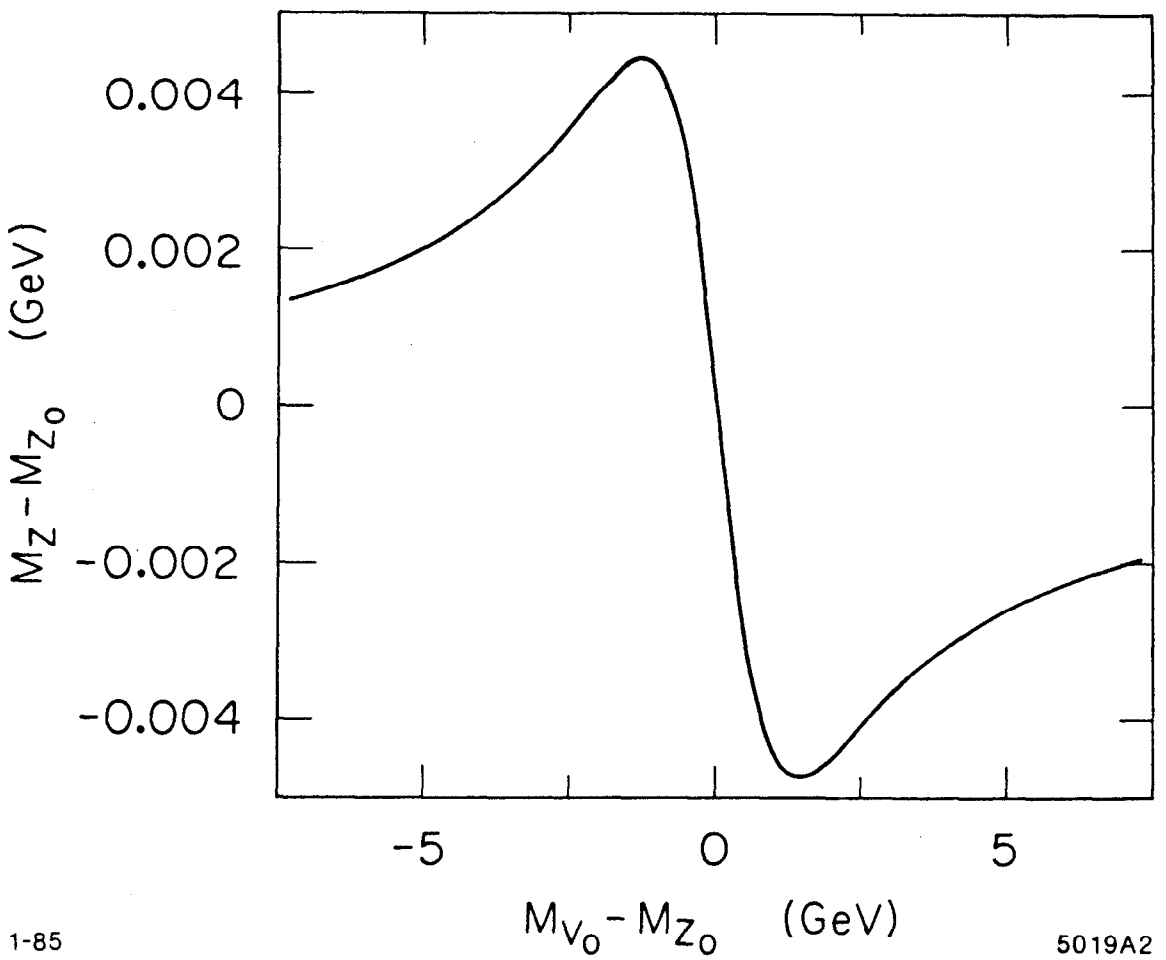

Figure 2. Change in the physical M_Z due to mixing.

the corresponding antifermions are forced to have opposite handedness). The couplings of the gauge bosons to fermions of charge Qe and third component of weak isospin T_{3L} are given in the standard model as

$$g_{z_0,L} = e\frac{T_{3L} - Q\sin^2\theta_W}{\sin\theta_W\cos\theta_W}$$

$$g_{z_0,R} = e\frac{-Q\sin^2\theta_W}{\sin\theta_W\cos\theta_W} \tag{2.19}$$

$$g_{\gamma,L} = g_{\gamma,R} = eQ,$$

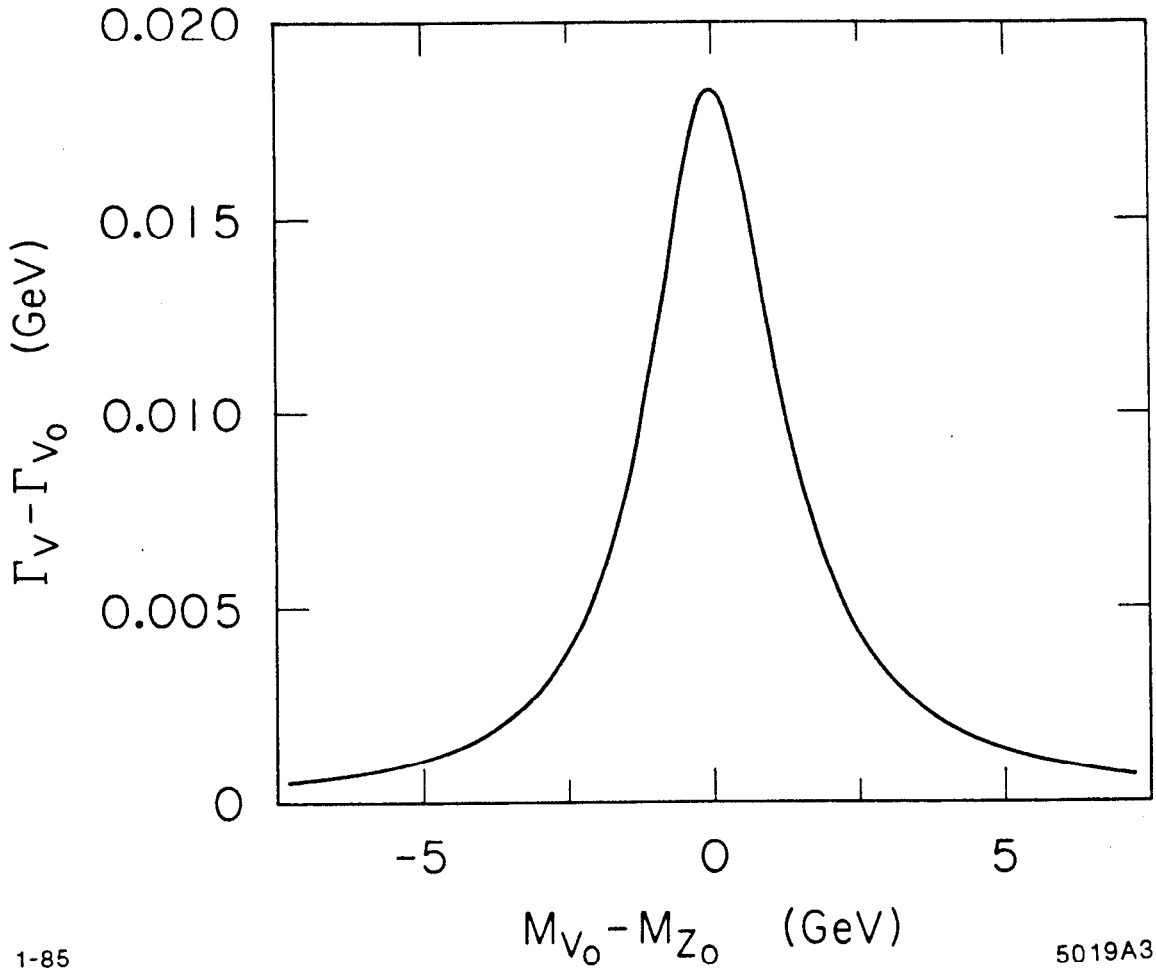

Figure 3. Change in the width of toponium.

while that induced by an intermediate virtual photon for the V_0 is

$$g_{V_0,L} = g_{V_0,R} = \frac{4}{3} e^2 Q \sqrt{3} (M_{V_0})^{-\frac{3}{2}} |\psi(0)|. \tag{2.20}$$

The angular dependence of the various amplitudes is given by standard arguments, so that the unpolarized cross section is

$$\frac{d\sigma(s,\theta)}{d\cos\theta} = \frac{s}{32\pi}\left[|A_{L,L}(s)|^2\left(\frac{1+\cos\theta}{2}\right)^2 + |A_{L,R}(s)|^2\left(\frac{1-\cos\theta}{2}\right)^2 + |A_{R,L}(s)|^2\left(\frac{1-\cos\theta}{2}\right)^2 + |A_{R,R}(s)|^2\left(\frac{1+\cos\theta}{2}\right)^2\right]. \tag{2.21}$$

Recalling $\sigma_{pt}(s) = 4\pi\alpha^2/3s$,

$$R(s) = \frac{\sigma(s)}{\sigma_{pt}(s)} = \frac{s^2}{64\pi^2\alpha^2}\left[|A_{L,L}(s)|^2 + |A_{L,R}(s)|^2 + |A_{R,L}(s)|^2 + |A_{R,R}(s)|^2\right]. \tag{2.22}$$

The value of R for $e^+e^- \to \mu^+\mu^-$ in the situation where M_{V_0} is 1 GeV below M_Z, which we arbitrarily choose for the purposes of illustration, is shown in Fig. 4. The dotted curve is with the Z alone, while the dashed line shows the case in which the couplings of the V_0 to initial and final fermions are set to zero. We find in this latter case that

$$R = \frac{(|g_{Z_0,L}|^2 + |g_{Z_0,R}|^2)_i(|g_{Z_0,L}|^2 + |g_{Z_0,R}|^2)_f}{64\pi^2\alpha^2}X = .1365\frac{\alpha^2(M_Z)}{\alpha^2(m_e)}X \tag{2.23}$$

in the case of $e^+e^- \leftarrow \mu^+\mu^-$, where

$$X = \left|\frac{s(s - M_{V_0}^2 + i\Gamma_{V_0}M_{V_0})}{(s - M_{V_0}^2 + i\Gamma_{V_0}M_{V_0})(s - M_{Z_0}^2 + i\Gamma_{Z_0}M_{Z_0}) - (\delta m^2)^2}\right|^2 \tag{2.24}$$

(doing the calculation in the unmixed basis).* While not visible in Fig. 4, the dashed curve does not precisely go through zero, but to $R \approx 5 \times 10^{-3}$, since we have made Γ_{V_0}=100 KeV and the zero of the amplitude is slightly off the real energy axis. The realistic case, including the photon intermediate state and bare

* The ratio of α^2's in Eq. (2.23) is about 1.15, and comes about because of the way the R-value is defined; see footnote 1.

V_0 couplings as per Eq. (2.20), is shown by the solid line. There still is a deep dip near M_{V_0}. A similar dip occurs for all the $^3S_1$ states below open top threshold, except that the effect occurs over a narrower energy region for the higher states since their widths (acquired mostly from mixing) are smaller. When $M_{V_0} > M_{Z_0}$ the dip occurs before the peak, rather than after it as in Fig. 4. For the very fortuitous case where $M_{V_0} = M_{Z_0}$, there is no peak at all; only a near zero right in the middle of the Z. Similar behavior is exhibited for $e^+e^- \to u\bar{u}$ and $e^+e^- \to d\bar{d}$.

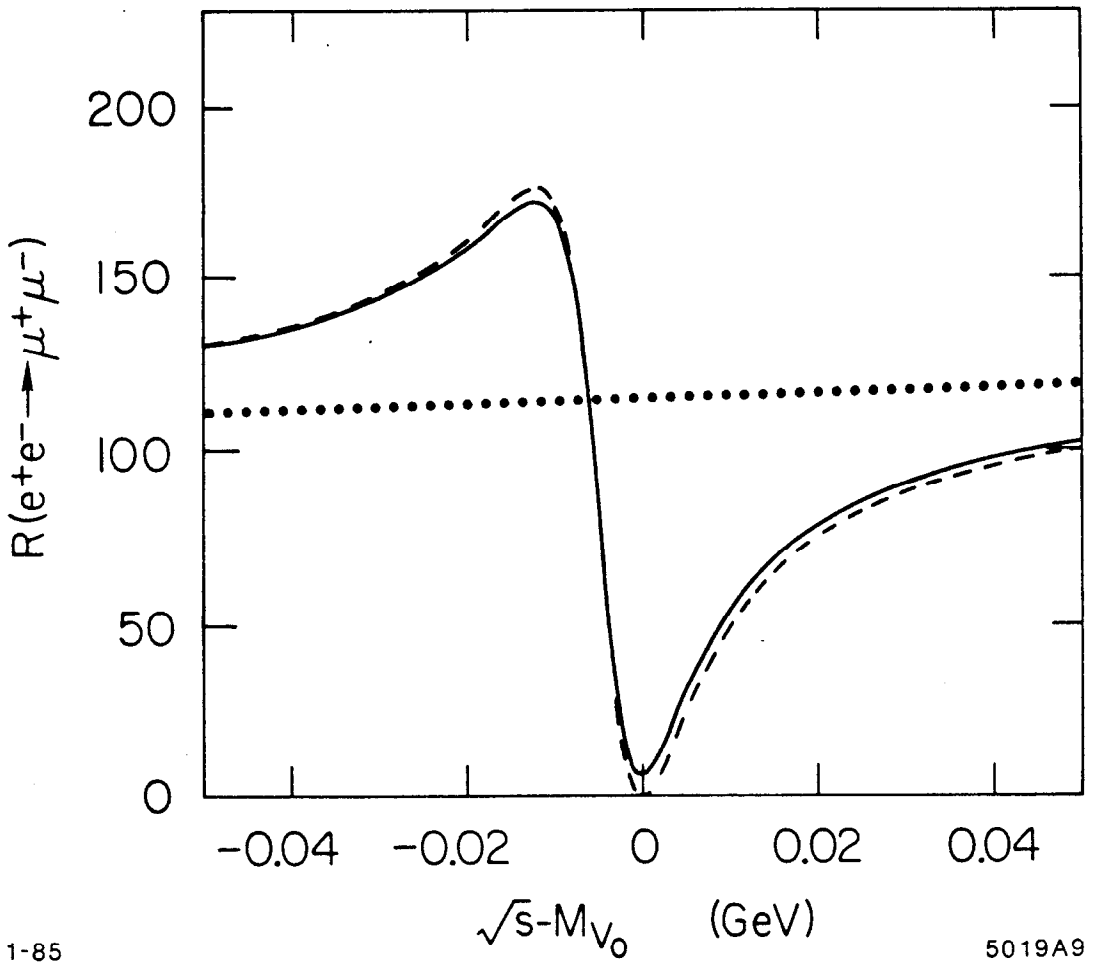

Figure 4. Effect of mixing in $R(e^+e^- \to \mu^+\mu^-)$.

Since we have the cross section in terms of amplitudes for fermions of definite handedness it is easy to find the expression for the longitudinal polarization (of the initial e^-) asymmetry:

$$A_{pol}(s,\theta) = \frac{A_1(s) + \frac{2\cos\theta}{1+\cos^2\theta} A_2(s)}{1 + \frac{2\cos\theta}{1+\cos^2\theta} A_{FB}(s)} \tag{2.25}$$

where

$$\begin{aligned} A_1 &= \frac{|A_{R,R}|^2 + |A_{L,R}|^2 - |A_{R,L}|^2 - |A_{L,L}|^2}{|A_{R,R}|^2 + |A_{L,R}|^2 + |A_{R,L}|^2 + |A_{L,L}|^2} \\ A_2 &= \frac{|A_{R,R}|^2 + |A_{R,L}|^2 - |A_{L,R}|^2 - |A_{L,L}|^2}{|A_{R,R}|^2 + |A_{L,R}|^2 + |A_{R,L}|^2 + |A_{L,L}|^2} \end{aligned} \tag{2.26}$$

and the front-back asymmetry

$$A_{FB} = \frac{|A_{R,R}|^2 + |A_{L,L}|^2 - |A_{L,R}|^2 - |A_{R,L}|^2}{|A_{R,R}|^2 + |A_{L,R}|^2 + |A_{R,L}|^2 + |A_{L,L}|^2}. \tag{2.27}$$

(The quantity A_{FB} used here has a maximum magnitude of unity. The more usual front-back asymmetry obtained by integrating over the forward and backward hemispheres, is a factor of 3/4 smaller.)

If we pay no attention to the angular distribution of the final state fermions and integrate over the center-of-mass scattering angle θ, then we are only sensitive to $A_1(s)$, which is sometimes referred to as "the" polarization asymmetry. For $e^+e^- \to \mu^+\mu^-$, $A_1(s) = A_2(s)$ and there is no distinction between them anyway. Fig. 5 displays the polarization asymmetry for the reaction $e^+e^- \to \mu^+\mu^-$ when M_{V_0} is 1 GeV less than M_{Z_0}. Again the dashed line gives the result when the bare V_0 has no coupling to the initial or final fermions. Since in this case the coupling of the V to the initial and final fermions comes entirely through mixing

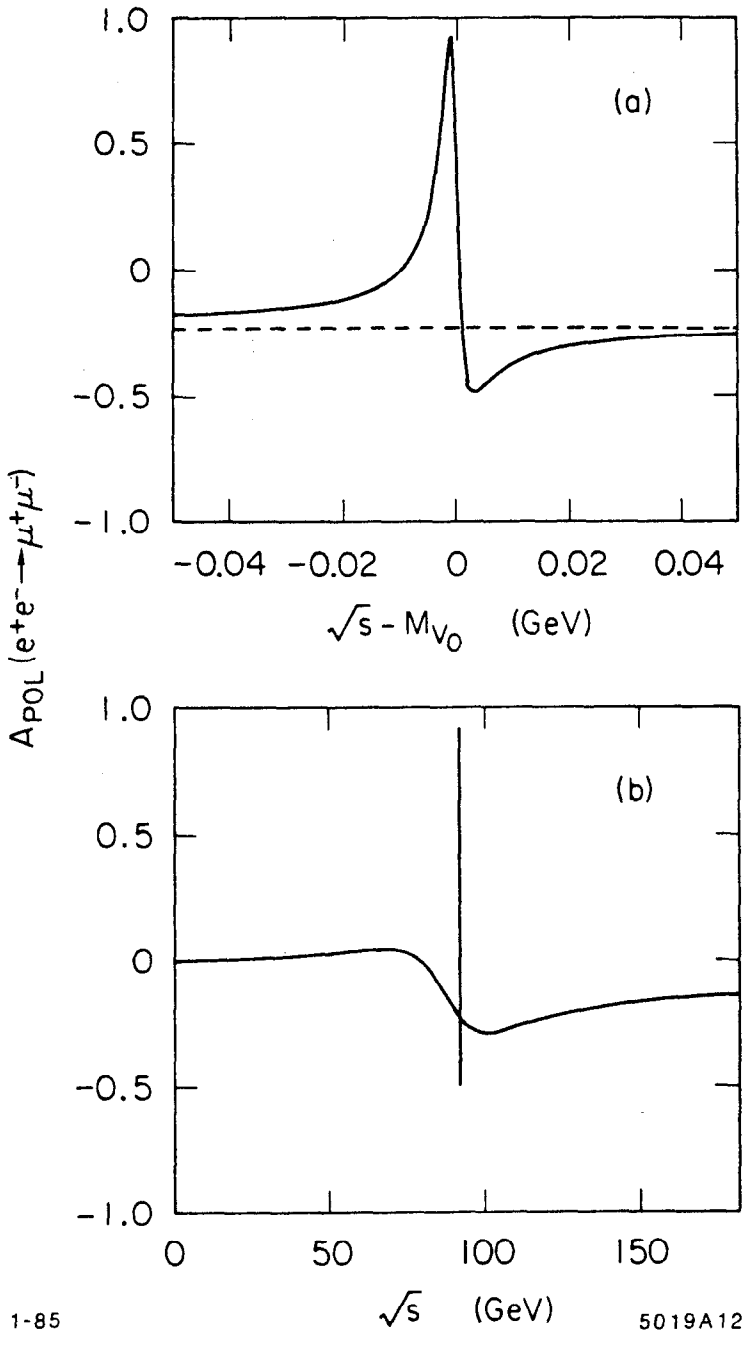

Figure 5. Effect of mixing on A_{POL} for $e^+e^- \to \mu^+\mu^-$.

with the Z_0, the ratios of its helicity couplings are identical to those of the Z and the value of A_{pol} is identical to that for the Z alone. However, when the amplitudes involving virtual photons are included (solid line in Fig. 5), the effects are dramatic. Although the amplitudes involving virtual photons are small, those coming from $V + Z$ also are small near M_{V_0} and one sees a large effect characteristic of the interference of the real part of the Breit-Wigner of the V with the rest of the amplitude.

Similarly, Fig. 6 shows the polarization asymmetries A_1 and A_2 in the vicinity of M_{V_0} for production of charge $\frac{2e}{3}$ and $-\frac{e}{3}$ quarks, u and d. Again one observes characteristic interference patterns due to the real part (e.g., in A_1 for $u\bar{u}$) and/or imaginary part (e.g., in A_2 for $d\bar{d}$) of the Breit-Wigner resonance amplitude of the V interfering with the rest of the amplitude due to $\gamma + Z$. The quark production amplitudes used in this computation do not include the contributions from strong interactions, *i.e.*, $V \rightarrow$ intermediate gluons $\rightarrow q\bar{q}$, which could in principle contribute further coherently interfering amplitudes, modifying the interference patterns. Similar comments hold for the forward-backward asymmetry shown in Fig. 7 for $\sqrt{s}$ in the neighborhood of M_{V_0}. As the asymmetries for $\gamma + Z$ alone do not vary strongly over the width of the Z, the general form of the asymmetry after the state V is introduced does not depend strongly on whether it is a few GeV below or above the Z mass.

The extension of the formalism to encompass mixing of the Z with an arbitrary number of toponium states is straightforward. For n states the mass matrix is (n+1)×(n+1):

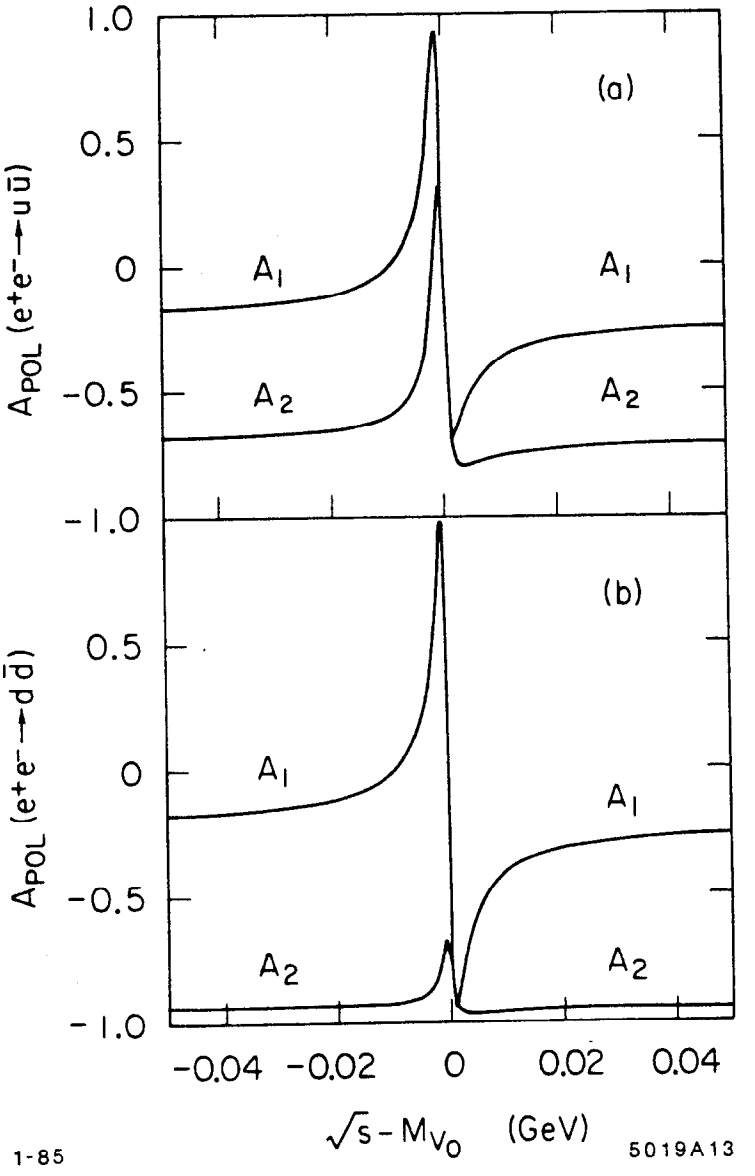

Figure 6. Effect of mixing on A_{POL} for $e^+e^- \to u\bar{u}$, $d\bar{d}$.

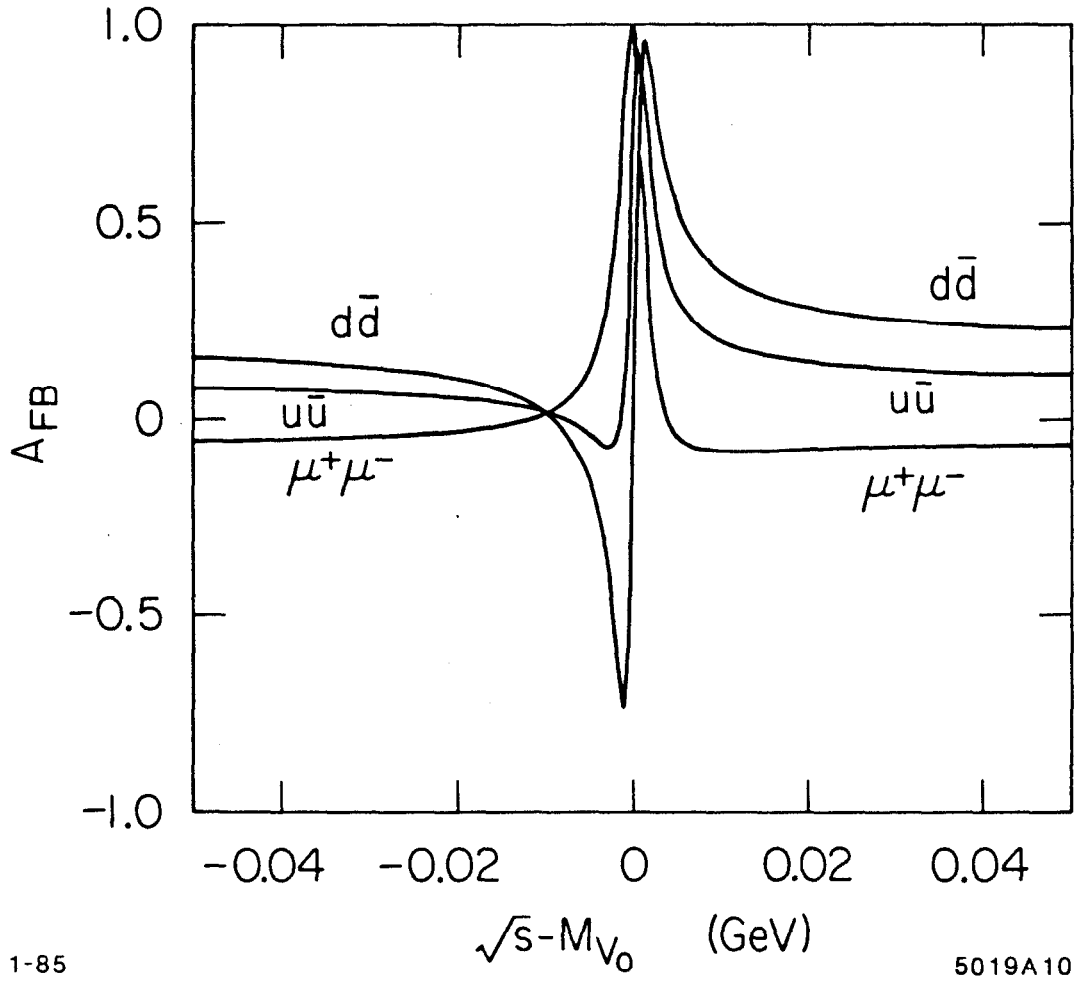

Figure 7. Effect of mixing on the forward-backward asymmetry.

$$M_0^2 = \begin{pmatrix} M_{Z_0}^2 - iM_{Z_0}\Gamma_{Z_0} & \delta m^2 & \delta m'^2 & \cdots \\ \delta m^2 & M_{V_0}^2 - iM_{V_0}\Gamma_{V_0} & 0 & 0 \\ \delta m'^2 & 0 & M_{V_0'}^2 - iM_{V_0'}\Gamma_{V_0'} & 0 \\ \vdots & 0 & 0 & \ddots \end{pmatrix} \tag{2.28}$$

where δm^2, $\delta m'^2$, ... parametrize the mixing between the Z and the spectrum of toponium states V, V', ... Mixing directly (e.g, through an intermediate photon) between toponium states is very small and has been neglected.

If one works only to second order in δm^2, $\delta m'^2$, ... then it is possible to write a simple expression for the rotation that diagonalizes M_0^2 and hence its eigenvalues and eigenvectors. We have found numerically that this gives a fair approximation to the masses and widths of the dressed states V, V', ..., and a good approximation to the cross sections. In our subsequent work we calculate in the unmixed basis, as the matrix can be inverted exactly. While this can be done analytically, it is easier to carry out the matrix manipulations numerically at each value of s.

Finally, above open top threshold two interesting effects occur. The bare width of the toponium states will no longer be negligible, changing the near zeroes in cross sections to minima where the cross section drops by less than an order of magnitude. Further, the mixing term δm^2 picks up an imaginary part as physical intermediate states are allowed ($V_0 \to T_i \bar{T}_i \to Z_0$), giving

$$\mathrm{Im}\delta m^2 = -\sum_i \sqrt{M_{Z_0}\Gamma_{Z_0\to T_i\bar{T}_i}}\,\sqrt{M_{V_0}\Gamma_{V_0\to T_i\bar{T}_i}}\,, \tag{2.29}$$

where the sum extends over all physical intermediate states (here T indicates a meson composed of the t quark and some lighter quark). In principle the imaginary part of δm^2 can be comparable to the real part, causing sizable changes in the interference.

3. Toponium Potentials

We shall be utilizing the spectrum of toponium states and their wave functions determined using the heavy quark potential of Richardson.[8] It has the advantages of correct long and short range behavior together with a minimal number of parameters. In addition it provides a very good set of predictions for the $^3S_1$ states of the upsilon system.[14] This potential is specified in momentum space by:

$$\widetilde{V}(q^2) = -\frac{4}{3}\,\frac{12\pi}{33-2n_f}\,\frac{1}{q^2\ln(1+q^2/\Lambda^2)}. \tag{3.1}$$

We use $n_f = 3$ (number of fermion species), since the relevant energy scale is the momentum of the bound quarks, which is less than, or around, the mass of the charm quark; furthermore, as this is a phenomenological potential, we wish to use the same parameters as did Richardson. It can be rewritten in position space as:

$$V(r) = \frac{8\pi}{33-2n_f}\,\Lambda\left(\Lambda r - \frac{f(\Lambda r)}{\Lambda r}\right), \tag{3.2}$$

where

$$f(t) = \left[1 - 4\int_1^\infty \frac{dq}{q}\,\frac{e^{-qt}}{[\ln(q^2-1)]^2+\pi^2}\right]. \tag{3.3}$$

We evaluate this potential numerically using[8] $\Lambda = .398\text{GeV}$, and then solve the radial Schrödinger equation,

$$u'' + \frac{2(l+1)}{r}u' + \frac{2\mu}{\hbar^2}\big[E - V(r)\big]u = 0, \tag{3.4}$$

where l is the angular momentum and $u(r)\cdot r^l = R(r)$, the radial wavefunction.

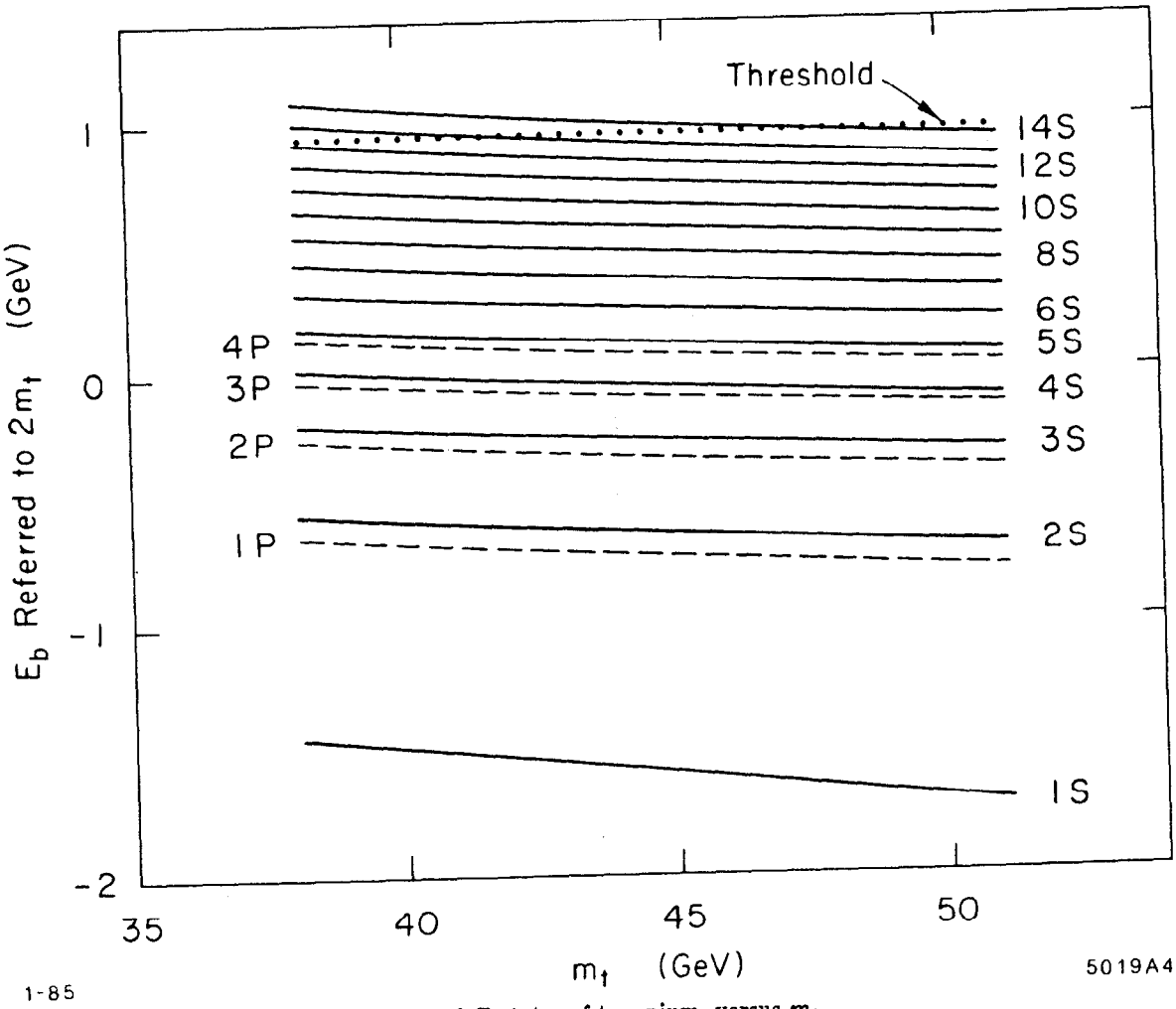

Figure 8. Binding energy of the S and P states of toponium, versus m_t.

The first several energy levels, as a function of the top quark mass, m_t, are shown in Fig. 8,[15] where $E_b = m_{t\bar{t}} - 2m_t$. The corresponding values of $\psi(0)=R(0)/\sqrt{4\pi}$, the wavefunction at the origin for the S states, are shown in Fig. 9. These wavefunctions are normalized with the condition

$$4\pi \int |\psi(r)|^2 r^2 dr = 1. \tag{3.5}$$

With this normalization the leptonic width (through an intermediate photon)

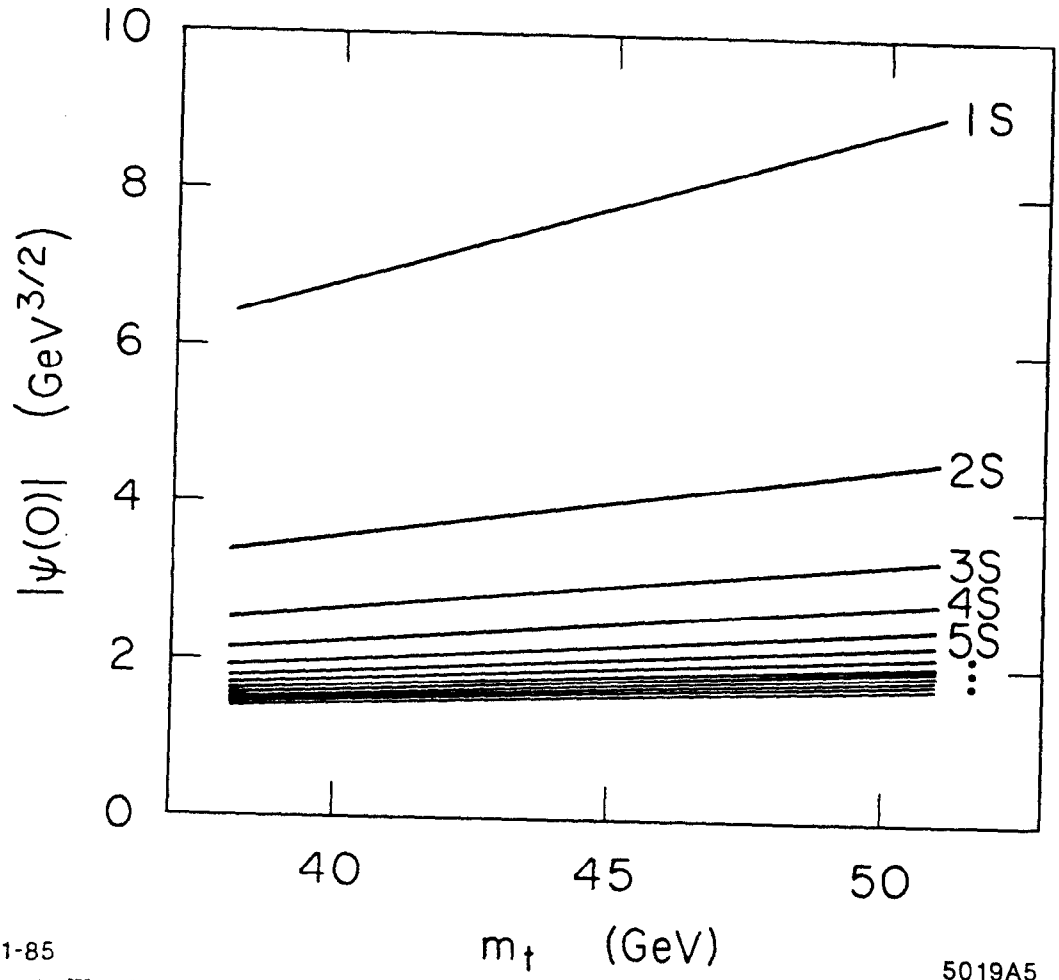

Figure 9. Wavefunction at the origin.

is[17,18]

$$\Gamma(V_0 \to e^+e^-) = \frac{16\pi\alpha^2}{M_{V_0}^2}|\psi(0)|^2 Q_t^2, \tag{3.6}$$

and corresponds to a leptonic width of about 9 KeV for the ground state.

To calculate where the threshold for bare top production occurs, we basically follow Eichten and Gottfried.[18] If we use the charm quark as a baseline we have

$$m_T - m_t = m_D - m_c + \frac{3}{4}(1 - m_c/m_t)\delta_c, \tag{3.7}$$

where the last term corrects for the hyperfine splitting between the D^* and D and between the T^* and T (the quantity $\delta_c = m_{D^*} - m_D$=.141 GeV). Inserting the mass of the charm quark appropriate to the Richardson potential (1.491 GeV), and the experimental D mass, yields $m_T - m_t = 0.477$ GeV. Alternately, we may use the bottom system as a baseline:

$$m_T - m_t = m_B - m_b + \frac{3}{4}(1 - m_b/m_t)\delta_b, \tag{3.8}$$

where now[19] $\delta_b = m_{B^*} - m_B$=.052 GeV. Again, inserting the quark mass appropriate to the Richardson potential ($m_b = 4.883$ GeV), we find $m_T - m_t = 0.425$ GeV.

The threshold is found at $2m_T$, i.e., .95 GeV+$2m_t$ or .85 GeV +$2m_t$ from Eq. (3.7) or Eq. (3.8), respectively. In Fig. 8 we have taken it to be at .95 GeV+$2m_t$ (indicated by the dotted line), with the result that there are 13 $^3S_1$ states below open top threshold for $m_t \approx 45$ GeV. Since the level spacing is about one $^3S_1$ state per hundred MeV near threshold, we would lose one such state to the continuum if we moved the threshold down to $2m_t + 0.85$ GeV.

4. Cross Sections and Asymmetries for Toponium Near the Z

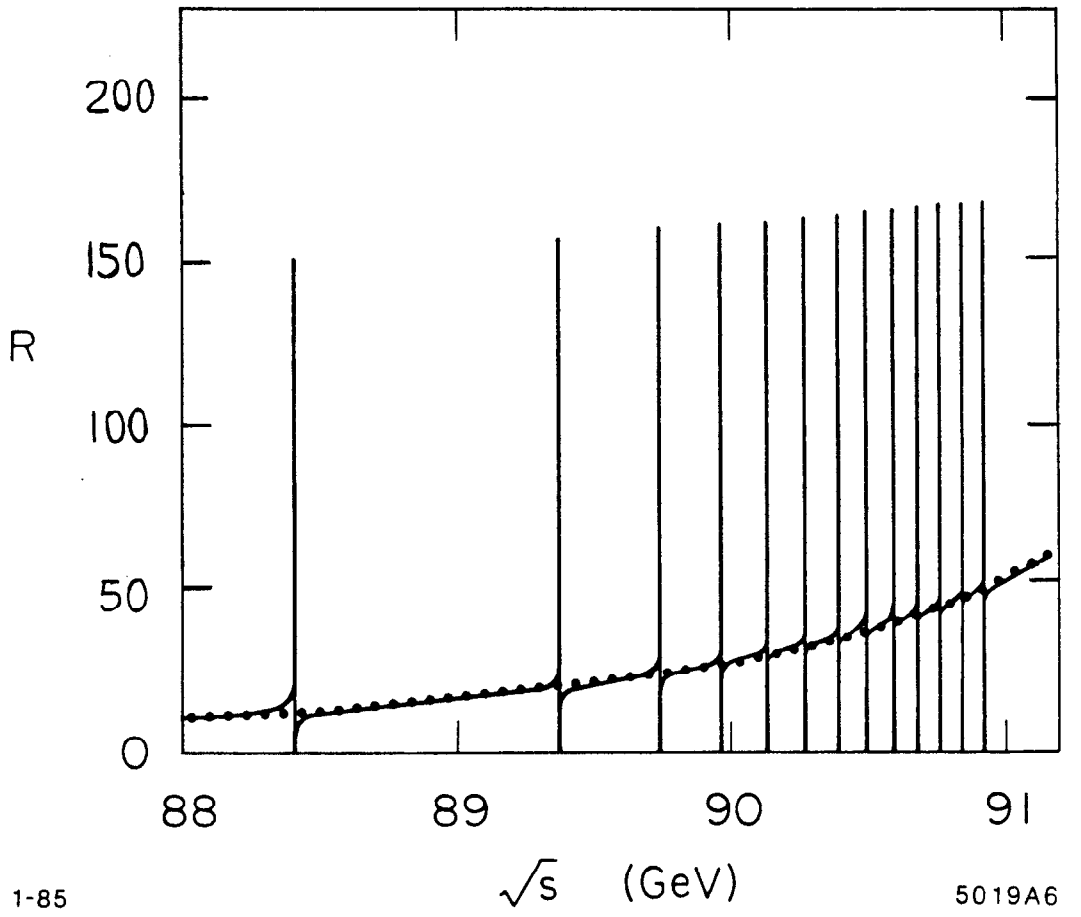

Figure 10. $R(e^+e^- \to \mu^+\mu^-)$, including mixing with several $t\bar{t}$ states; m_t=45 GeV.

We are now in a position to put together the mixing formalism in Section 2 with the toponium spectrum and functions of Section 3. Indeed, for the ground state of toponium we have already done this in that we explored the consequences of the mixing formalism by using it as an example in Section 2 for mass shifts, cross sections, and asymmetries in the two state system consisting of the 1S state, V_0, and the Z_0. Figures 10, 11, and 12 show the cross section in the neighborhood of the Z, for $e^+e^- \to \mu^+\mu^-$, normalized to $\sigma_{pt} = 4\pi\alpha^2/3s$, for

situations where m_t=45, 47, and 49 GeV respectively. In each case the distinct interference pattern of each of the thirteen $^3S_1$ states assumed to be below open top threshold is visible. As we move over the peak of the Z the peak-dip order in the interference changes to dip-peak.

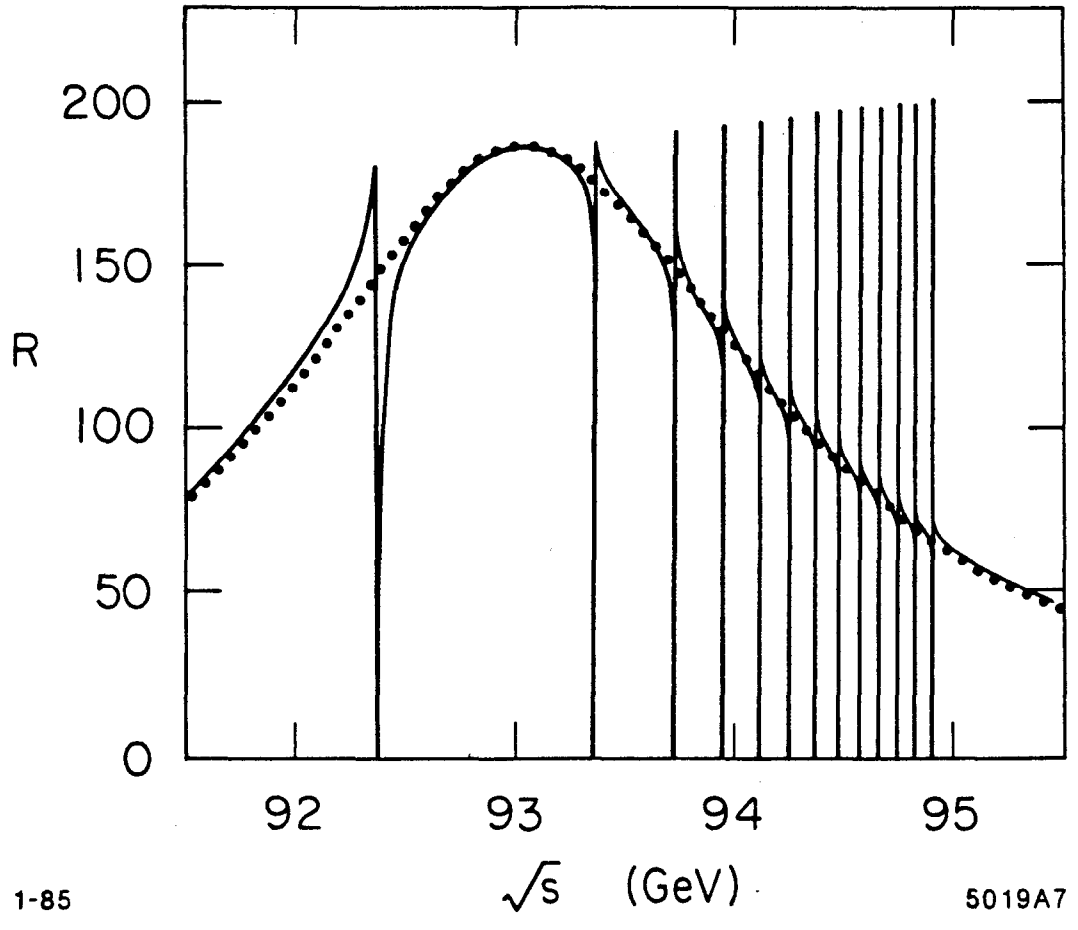

Figure 11. $R(e^+e^-\to\mu^+\mu^-)$, including mixing with several $t\bar{t}$ states; m_t=47 GeV.

The width (acquired by mixing) of the toponium states decreases as we go to higher energy levels because the wave function at the origin (see Fig. 9) decreases, and so proportionally does the amplitude for mixing with the Z. However, the height of the peak (in R) remains approximately the same. In fact, the peaks of

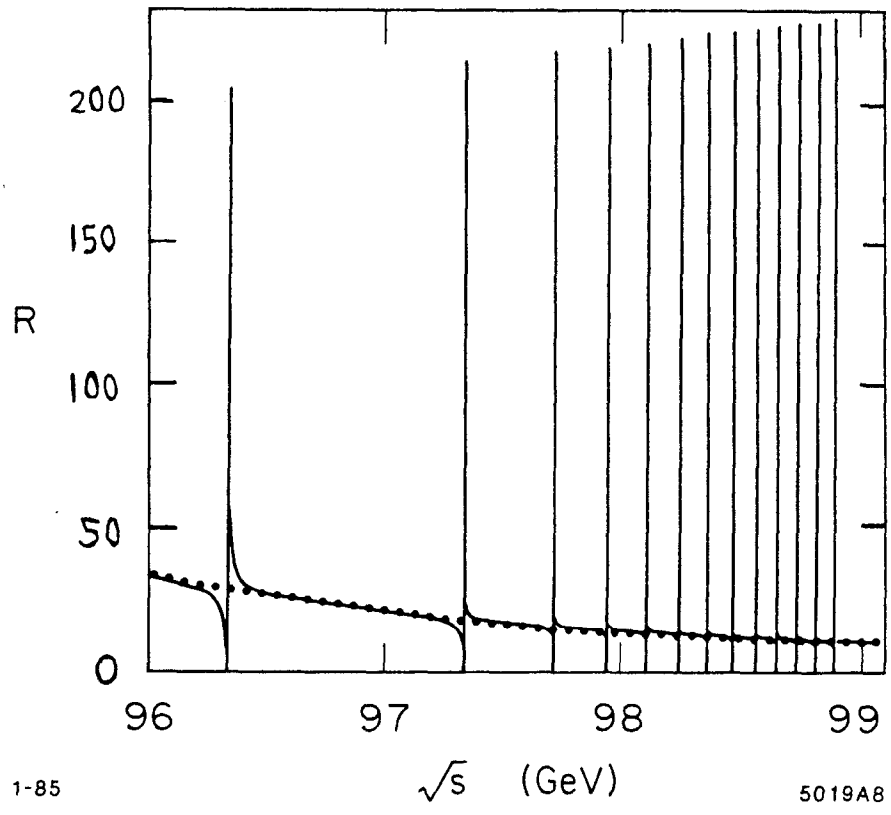

Figure 12. $R(e^+e^-\to\mu^+\mu^-)$ including mixing with several $t\bar{t}$ states; m_t=49 GeV.

the V_0 resonances, as well as that of the Z_0, fall on a very slowly varying curve. This behavior is exactly correct for a resonance, V, which acquires all its width from mixing with the Z, for from Eq. (2.23) we have

$$R = \frac{s^2(|g_{Z_0,L}|^2 + |g_{Z_0,R}|^2)_i(|g_{Z_0,L}|^2 + |g_{Z_0,R}|^2)_f}{64\pi^2\alpha^2\left|s - M_{Z_0}^2 + i\Gamma_{Z_0}M_{Z_0} - \frac{(\delta m^2)^2}{s-M_{V_0}^2}\right|^2}. \tag{4.1}$$

This is a maximum for a value of s (very close to $M_{V_0}^2$) for which the real part of the quantity $(s - M_{Z_0}^2 + i\Gamma_{Z_0}M_{Z_0}) - \frac{(\delta m^2)^2}{s-M_{V_0}^2}$ vanishes. At that point,

$$R_{peak} = \left(\frac{s_{peak}}{M_{Z_0}^2}\right)^2 \frac{M_{Z_0}^4(|g_{Z_0,L}|^2 + |g_{Z_0,R}|^2)_i(|g_{Z_0,L}|^2 + |g_{Z_0,R}|^2)_f}{64\pi^2\alpha^2|i\Gamma_{Z_0}M_{Z_0}|^2}$$
$$= \left(\frac{s_{peak}}{M_{Z_0}^2}\right)^2 R_{peak,Z_0} \approx \left(\frac{M_V}{M_Z}\right)^4 R_{peak,Z} \qquad (4.2)$$

Once we are above open top threshold, the situation changes considerably. The width of an unmixed toponium state presumably becomes tens of MeV, as is the case for the Ψ'' and Υ'''. The peak and dip structure from interference with the Z is much less dramatic in $e^+e^- \to \mu^+\mu^-$, as is shown in Fig. 13.

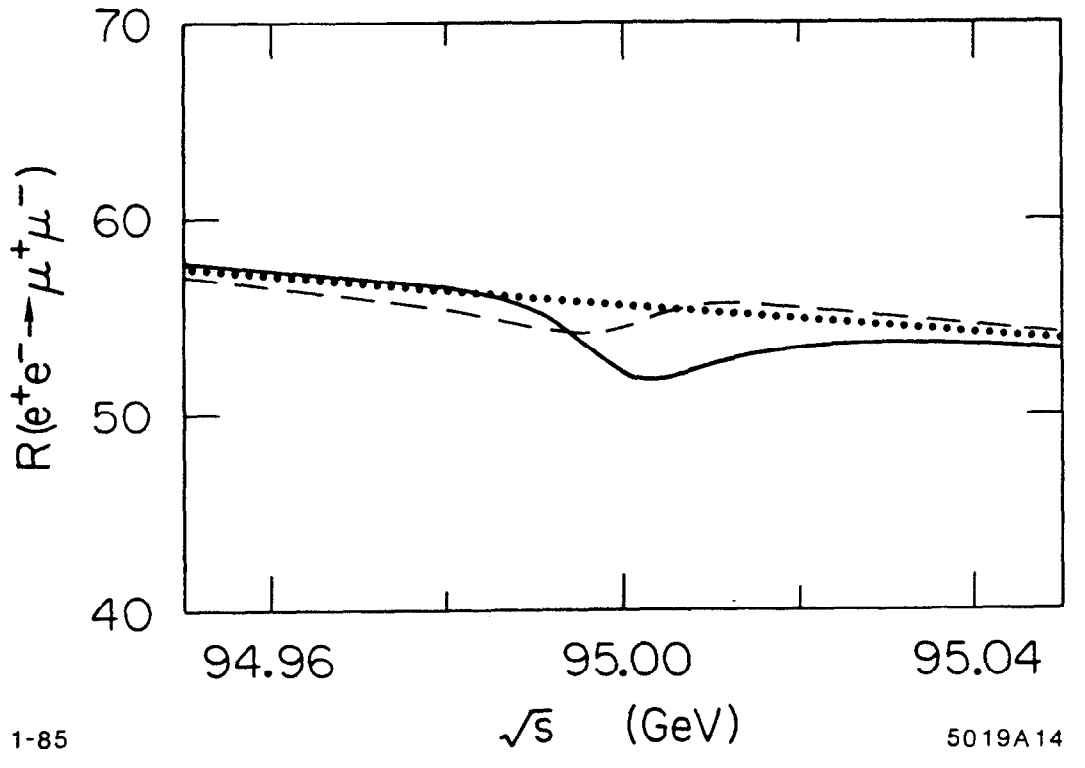

Figure 13. $R(e^+e^- \to \mu^+\mu^-)$ for a 14S state of toponium.

Here we have illustrated the situation by taking the 14^3S_1 state to be 2 GeV above

the Z and to have a width of 20 MeV for decay into pairs of open top states. The dashed line shows the case of real δm^2 while the solid line indicates what happens when there is an imaginary part of the same magnitude (but opposite sign), which is a plausible possibility from Eq. (2.29). Again, the dotted line is the Z alone for comparison. The imaginary part of δm^2 makes the interference pattern somewhat more impressive but when we note the suppressed zero for the vertical axis in Fig. 13 it is clear that in any case for $e^+e^- \to \mu^+\mu^-$ we have a much less impressive effect than that for a resonance below threshold. Of course, if we look at $e^+e^- \to t\bar{t}$, we will see a much greater effect, for $t\bar{t}$ is the major decay of such a resonance while $\mu^+\mu^-$ is a very minor one. However, once we are above open top threshold the situation becomes quite complicated in that different states will mix with each other as well as the Z and the approximation inherent in producing zeroes in the mass matrix in Eq. (2.28) breaks down. At the same time all the mixing matrix elements become complex. While interesting, a detailed investigation is beyond the scope of this thesis.

The situation with respect to the polarization or front-back asymmetries when we include the whole spectrum of $^3S_1$ toponium states is very much an iteration of what is found in Figs. 5, 6, and 7 for the 1S state. Of course, there are small variations as the t quark mass is changed and the "background" asymmetries due to the γ and Z change, but the general form of the interference pattern remains the same as we move over the peak of the Z. Again as we go to higher radial excitations, the width of the mixed toponium states decreases (to $\lesssim 1$ MeV just below threshold) making the measurement of these large swings in the asymmetries very difficult.

This brings us to the question of how much of this is in fact measurable under actual experimental conditions where the spread in beam energy is not negligible. To see how this affects the results we have taken the curve in Fig. 11 (corresponding to m_t=47 GeV), which would be the measured cross section with no beam energy spread, and smeared it with a Gaussian corresponding to $\sigma_{E_{\rm beam}} = 40$ MeV (*i.e.*, $\sigma_E/E \approx 0.8\times10^{-3}$) and to $\sigma_{E_{\rm beam}} = 100$ MeV (*i.e.*,$\sigma_E/E \approx 2\times10^{-3}$). The result is shown by the solid and dashed line respectively, in Fig. 14; the dotted line is the Z alone.

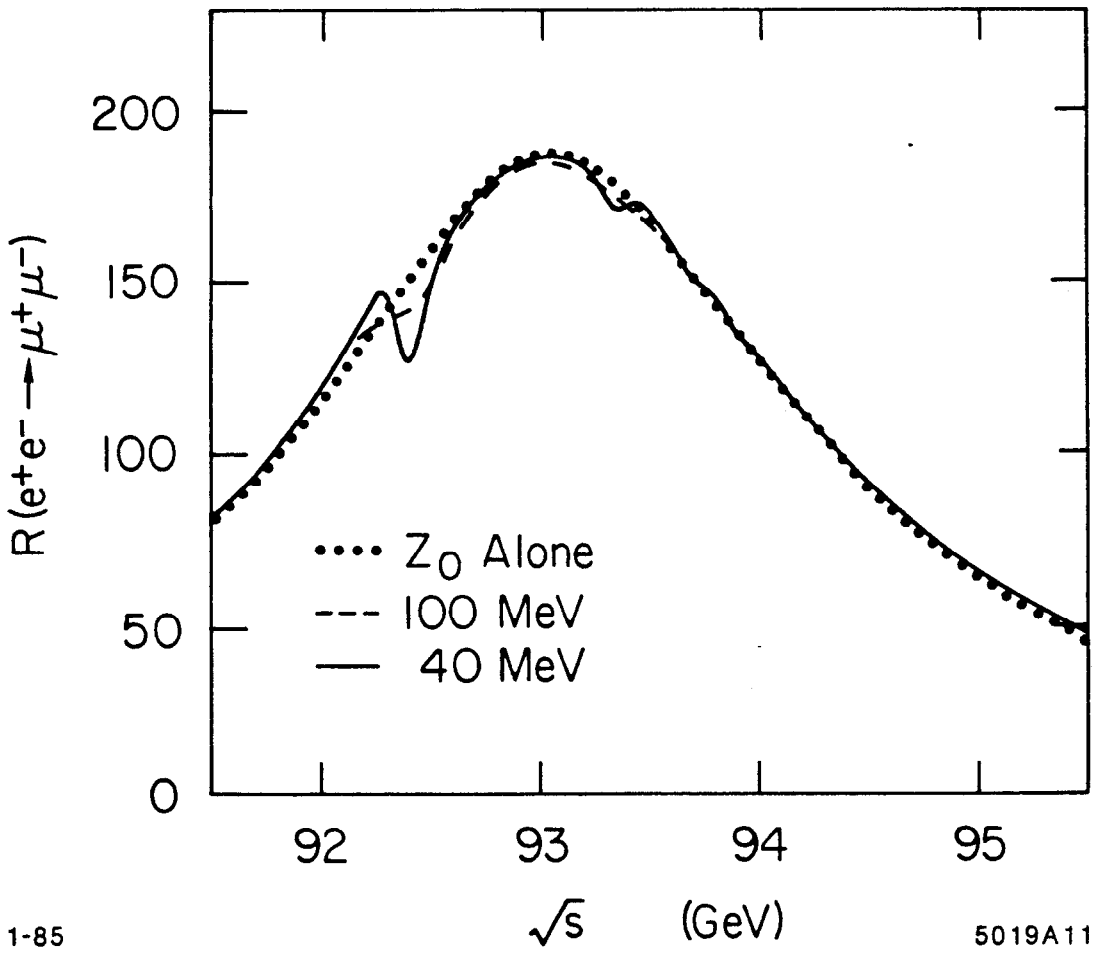

Figure 14. $R(e^+e^-\to\mu^+\mu^-)$ smeared, for $\sigma_{\rm beam}$ = 40, 100 MeV.

The latter case is presently the specification for the SLC, although the former case, which is roughly nominal LEP performance without wigglers, is also achievable[20] at SLC. In the latter case the structure due to the higher ${}^3S_1$ states is washed out and we can only see a mild undulation due to the 1S state, instead of the deep dip in Fig. 4. In the former case, with a narrower beam spread, the ground state is quite clear and a few higher states can be picked off from their interference pattern with the Z.

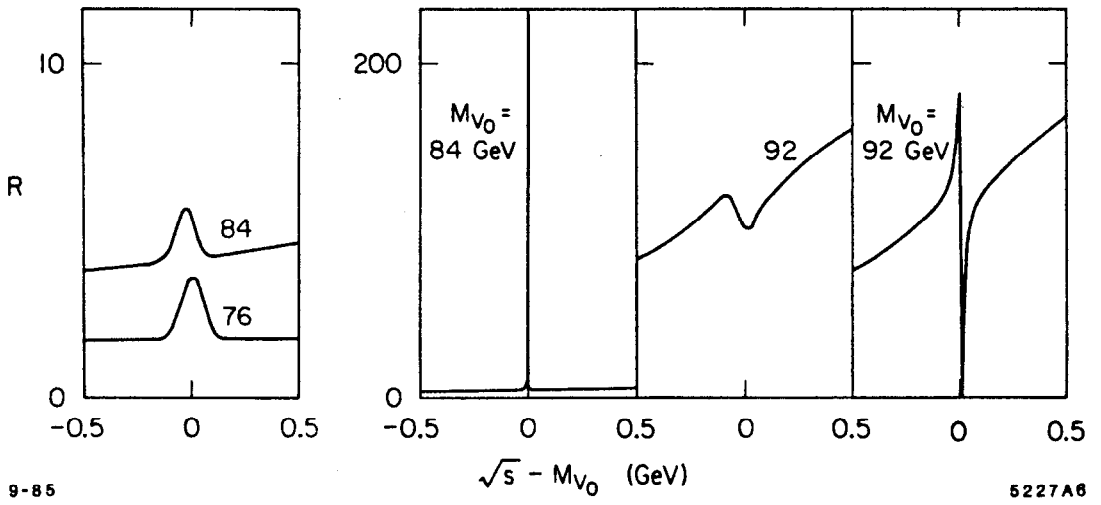

Figure 15. $R(e^+e^- \to \mu^+\mu^-)$ smeared ($\sigma_{\text{beam}} = 40$ MeV) and not, for $M_{V_0} = 76$, 84 and 92 GeV.

We remark that even for a V relatively far away from the Z, the enhancement due to mixing should be quite noticeable (see Fig. 15). The height of the peak does not decrease, though its width does. The smeared height is therefore greatly

reduced, but should be compared to the also much reduced background due to the Z. Note that to get comparable statistics to those obtained on the Z, one must run for far longer.

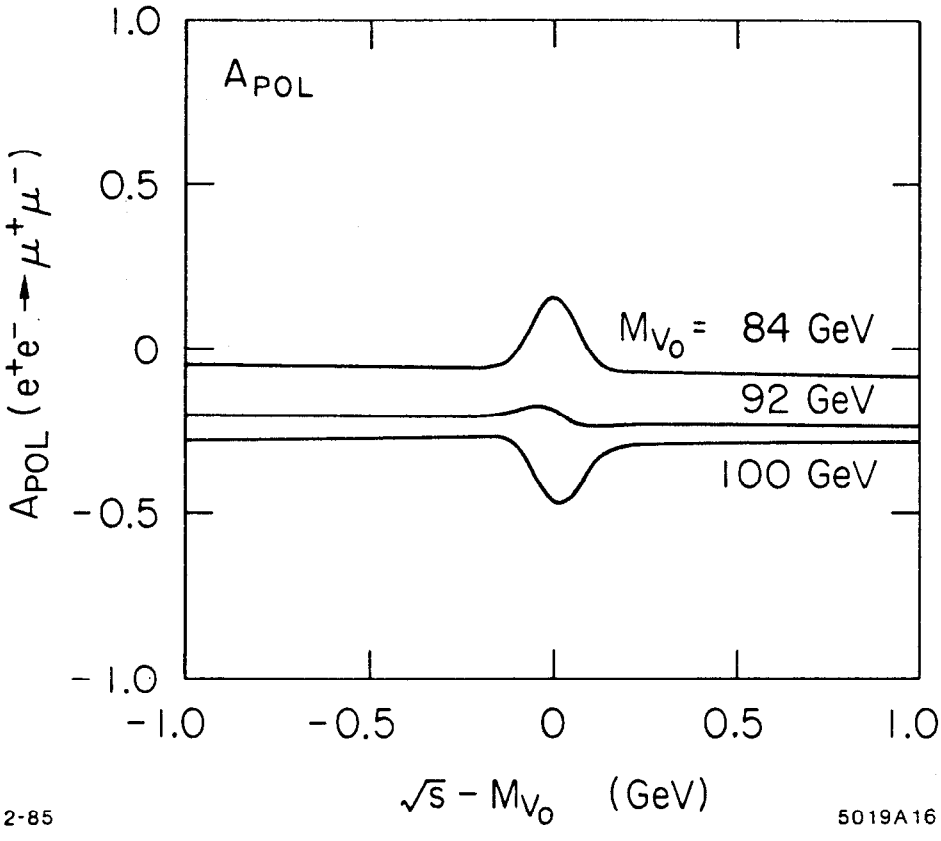

Figure 16. A_{POL} smeared, for various M_{V_0}.

The effects of smearing with $\sigma_{E_{\rm beam}}$=40 MeV on A_{pol} and A_{FB} are shown for the ground state of toponium in Figs. 16 and 17, respectively. Part of the reason these asymmetries have such a small variation when M_{V_0} is near M_Z (e.g. M_{V_0} =92 GeV in the figures), is that the unpolarized cross section due to the Z (which occurs in the denominator of the expression for the asymmetries) is large there. Even with the smearing one has fairly sizable effects in the asymmetries

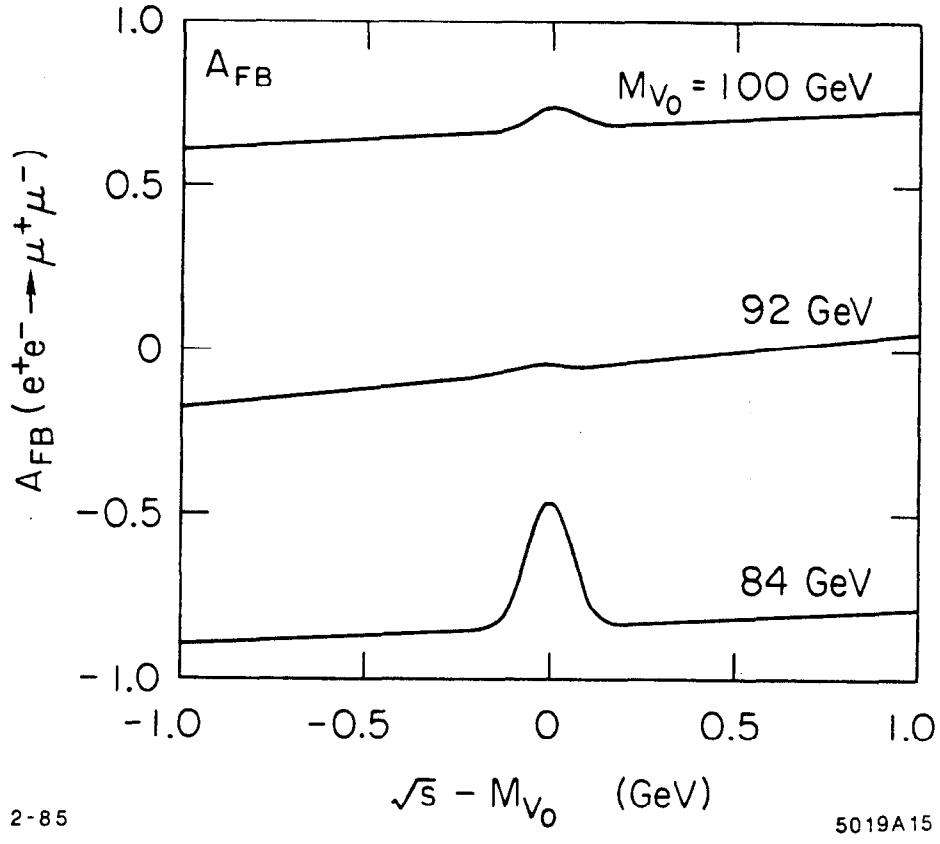

Figure 17. A_{FB} smeared, for various M_{V_0}.

well below[21,22] or well above the Z.

Thus with $\sigma_{E_{\rm beam}} \approx 40$ MeV one should be able to see quite distinctive indications for the first few levels of toponium both in the cross section and the polarization and front-back asymmetries. Even with $\sigma_{E_{\rm beam}} \approx 100$ MeV, if Nature is kind enough to put toponium near the Z, the effects due to interference of the ground state with the Z are visible, and they are capable at least of giving us information on the properties of the t quark and in particular, fairly precise knowledge of m_t and hence of where to look for open top threshold.

5. Toponium and two-Higgs models

In this chapter we would like to move away from toponium temporarily, and discuss some of the phenomenology of a model with an extended Higgs sector, specifically models with two Higgs doublets, although much of what we will discuss can be generalized to include more doublets. The new particles are two charged and two neutral bosons; an additional parameter is the vacuum expectation value (VEV) of the new doublet—or, equivalently, the ratio of the VEV's of the two doublets, if we fix an appropriate combination to be that of the standard model. Changing this VEV ratio changes the strength of the physical Higgs couplings and hence the size of the effects of the additional bosons; current physics, through the experimental absence of these effects, places limits on allowable values of the VEV ratio.

One first requires that flavor-changing neutral currents (FCNC) be absent at tree level. This can be done by imposing a discrete symmetry that forbids certain Higgs couplings. One scheme[24] requires one Higgs doublet to couple only to up-type quarks (i.e., u, c, and t) and the other only to down-type quarks. Thus, for each set of quarks, a single Higgs doublet is responsible for both mass matrix and neutral Higgs couplings, so, as in the standard model, the two matrices diagonalize simultaneously and FCNC are absent at tree level. Another scheme[25] allows only one Higgs doublet to couple to quarks at all, so that again the mass and coupling matrices diagonalize simultaneously.

We begin by discussing bounds on masses and couplings (VEV ratios) of charged Higgs bosons that follow from their effects on neutral B meson mixing.

We compare these bounds to those derived from the $K_S^0 - K_L^0$ difference,[26] and to those derived, with additional assumptions, from CP-violating effects in the K system.[27] We then consider what effects neutral-Higgs boson exchange might have on toponium physics. The Higgs exchange adds an attractive term to the interquark potential, which, for allowed values of the relevant parameters, can have dramatic effects on the spectrum and wave functions of toponium. However, distinguishing these effects from the variations of different, but theoretically acceptable, potentials, can present a problem.

5.1 LIMITS FROM $B^0 - \bar{B}^0$ MIXING

The three box diagrams contributing in lowest order to $B^0 - \bar{B}^0$ mixing are shown in Figure 18. The first is the standard model contribution. The other two can only occur in a model with more than one Higgs doublet, as H is the physical, charged Higgs. The t quark contribution dominates the expression for the mass difference, since it is weighted by Kobayashi-Maskawa (KM) angle factors whose magnitudes are similar to those for the charm quark, while $m_t^2 >> m_c^2$. Thus we expect much tighter bounds than those found in the K-meson system; additionally, the freedom in choosing matrix elements, and in KM angle related factors is considerably smaller than in the K-meson system.

CLEO, at the e^+e^- storage ring CESR, observes B_d^0 and $\overline{B}_d^0$ mesons pair produced near threshold, *i.e.*, without other particles. Their decay amplitudes are therefore coherent, and the like sign to opposite sign dilepton ratio is equal to the "wrong"-sign lepton to "right"-sign lepton ratio for a single B meson. This

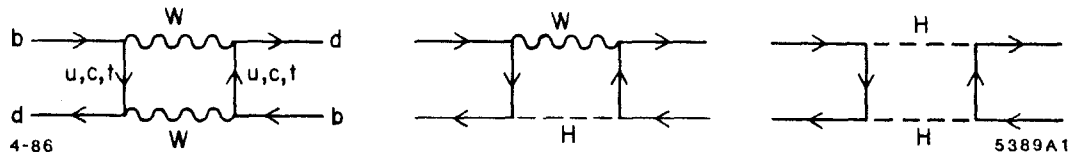

Figure 18. Box diagrams contributing in lowest order to $B^0-\bar{B}^0$ mixing .

can be written as follows (neglecting effects of possible CP violation)

$$r = \frac{N(l^+l^+) + N(l^-l^-)}{N(l^+l^-) + N(l^-l^+)} = \frac{\Gamma(B^0 \to l^- + \cdots)}{\Gamma(B^0 \to l^+ + \cdots)} = \frac{(\Delta M/\Gamma)^2}{2 + (\Delta M/\Gamma)^2} \tag{5.1}$$

where $\Delta M = M_S - M_L$ and $\Gamma = (\Gamma_L + \Gamma_S)/2$. CLEO's published upper limit on the mixing corresponds to

$$r < 0.30 \tag{5.2}$$

which translates to the bound

$$|\Delta M/\Gamma| < .93. \tag{5.3}$$

This bound uses the assumption $\tau_{B^0} = \tau_{B^\pm}$. Recently reported data could be interpreted as improving the bound, or as loosening the lifetime constraint.

Neglecting the $H - W$ diagram, and approximating the loop integrals, we find

$$\Delta M = \frac{G_F^2 f_B^2 m_B B_B s_1^2 s_2^2 m_t^2}{6\pi^2} \left[1 + \frac{1}{4}\left(\frac{\xi}{\eta}\right)^4 \frac{m_t^2}{M_H^2}\right], \tag{5.4}$$

where ξ/η is the VEV of the Higgs doublet coupling to the up-type quarks

divided by that of the doublet coupling to down-type quarks. Here m_B is the B meson mass, s_1 is the sine of the first KM angle, and m_t is the t quark mass; f_B is defined analogously to the pion and kaon decay constants, f_π and f_K; B_B is the bag factor for the B meson, and s_2 is the sine of the second KM angle. The first four parameters are fairly well-determined; we take $m_B = 5.3$ GeV, $s_1 = .23$, $f_B = f_K = .16$ GeV and $m_t = 45$ GeV (m_t could be larger, but this would only make our bound better, and it cannot be much smaller; we absorb any uncertainty in f_B into B_B).

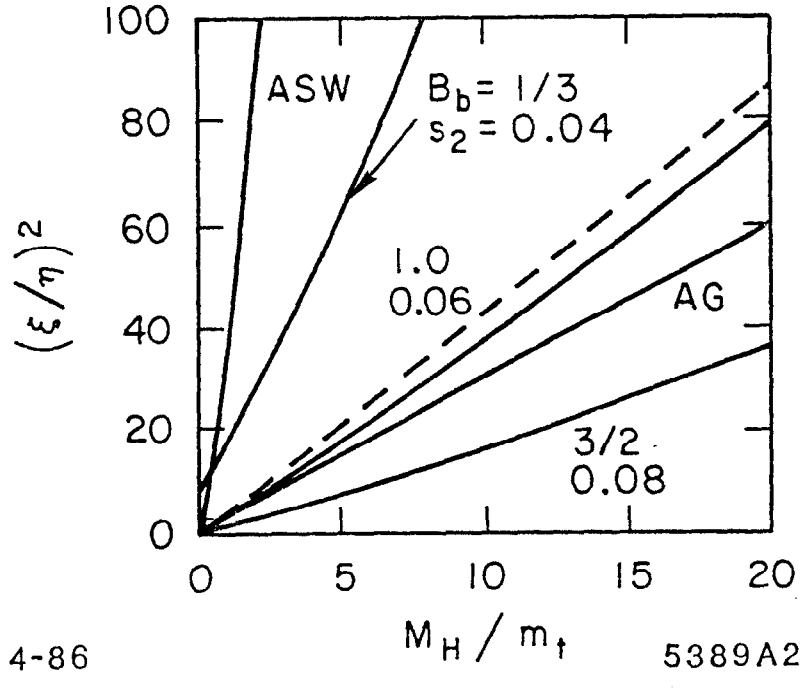

Figure 19. Limits on $(\xi/\eta)^2$ versus charged-Higgs-boson mass.

Fig. 19 shows our limit for various values of the bag factor and s_2. As "reasonable" parameters we pick $B_B = 1$ and $s_2 = 0.06$. The dashed line is the above, approximate calculation, while the solid line is the limit resulting if we evaluate the loop integrals exactly, and include the Higgs–W cross term. I also show our limits for the conservative values $B_B = 1/3$ and $s_2 = 0.04$, and for the "optimistic" values $B_B = 3/2$ and $s_2 = 0.08$—or equivalently, for improved experimental limits on $B^0 - \bar{B}^0$ mixing. For comparison, we show two previously calculated limits: the first, labeled ASW,[26] is the limit from $K\bar{K}$ mixing in the four quark model, and the second, labeled AG,[27] is the limit determined by considering CP violation in the neutral K system. While this second bound is comparable to ours, it requires the additional assumption that the primary contribution to the CP violation parameter ϵ be from the $W - W$ diagram, rather than from those involving the Higgs, which may not be true.

With the unitarity constraint that the Higgs mass be less than of order 1 TeV, we have an Higgs-mass-independent bound of

$$\frac{\xi}{\eta} \lesssim 10 - 15. \tag{5.5}$$

5.2 Effects of allowed two-Higgs models on toponium physics

The neutral-Higgs (H_0) exchange contributes to the toponium potential, with the H_0 coupling enhanced by the ratio ξ/η (we ignore possible mixing effects between the different neutral Higgs).

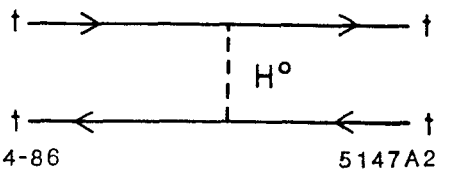

Figure 20. Higgs contribution to toponium potential.

The new term is an attractive Yukawa, in momentum space

$$-\left(\frac{\xi}{\eta}\frac{g}{2}\frac{m_t}{M_W}\right)^2 \frac{1}{M_H^2+q^2} \quad \text{or} \quad -\left(\frac{\xi}{\eta}\frac{g}{2}\frac{m_t}{M_W}\right)^2 \frac{e^{-rM_H}}{4\pi r} \tag{5.6}$$

in coordinate space. This has the effect of increasing the wavefunction at the origin, since it pulls in the wavefunctions, and of lowering energy levels (increasing binding energies). It also increases the level spacings, since it affects the lowest lying states the most. The number of states below threshold could change, but not significantly, since states above the 3S are almost unaffected (this will be an unobservable effect, since with the expected resolution of SLC or LEP, we only hope to see the first 2 to 5 states out of the 11 to 13 states below threshold). Other quarkonia are, in principle, affected, though negligibly, due to their light mass.

Let us now consider the $2S/1P$ splitting. A theorem due to Martin[29] states that if $\Delta V(r) > 0$ (true for all proposed quarkonia potentials), the nS state lies above the (n-1)P state, while if $\Delta V(r) < 0$ for all r such that $dV/dr > 0$ (true for the Higgs potential), the nS state lies below the corresponding P state. Here we

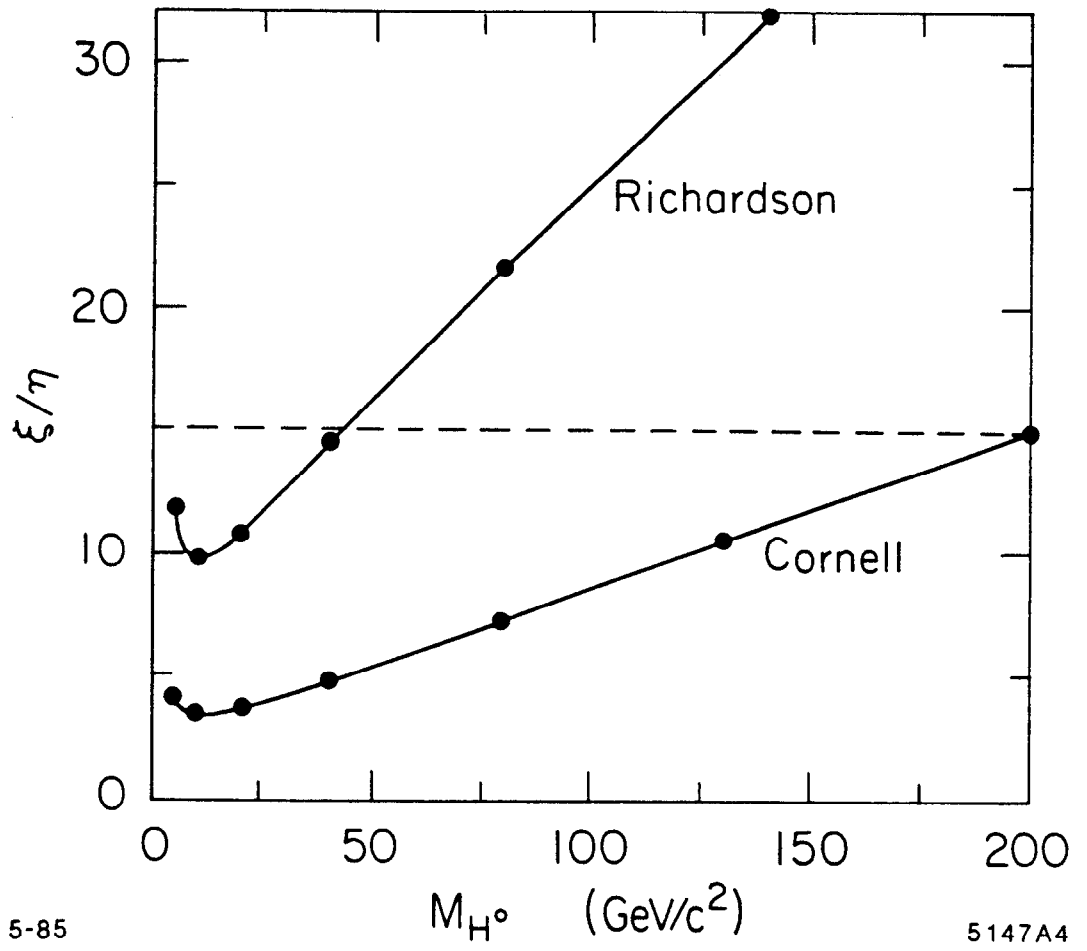

Figure 21. Minimum value of ξ/η for which level inversion occurs.

have a qualitative signature of the presence of the Higgs. However, the theorem requires a given condition on $\Delta V(r)$ to hold for all r. (The condition $dV/dr > 0$ holds for all r, for both potentials.) What happens when the Higgs dominates only near the origin? We might guess that relevant energy levels will be inverted if the Higgs term dominates below some relevant radius, perhaps that of the 2S or 1P. As M_H increases, the range of the Higgs potential decreases and we need a larger value of ξ/η to keep $\Delta V < 0$. This does give a qualitative picture of what happens. We find, numerically, the value of ξ/η at which $E_{2S} = E_{1P}$, shown

in Fig. 21 for two different potential models.[30] The dashed line indicates the charged-Higgs-mass independent bound of the previous section. Level inversion occurs for points in parameter space above the curves shown.

We can make a semi-quantitative analysis of the wavefunction change by examining the singular part of the potentials. This goes from $-c/r$, where c is some potential-model-dependent constant, to

$$-\left(c+\left(\frac{\xi}{\eta}\frac{g}{2}\frac{m_t}{M_W}\right)^2\frac{1}{4\pi}\right)\frac{1}{r}\,. \tag{5.7}$$

But $|\psi(0)|^2 \propto (c\ m_t)^3$ for a Coulomb potential, so we expect the dependence

$$|\psi(0)|^{2/3} = |\psi(0)|^{2/3}_{\xi/\eta=0}\left[1+a(\xi/\eta)^2\right], \tag{5.8}$$

where the constant a is deduced from Eq. (5.7). Numerically, we find this behavior for small ξ/η (5 to 10), although a is smaller than calculated from Eq. (5.7), because of the screening effect of the factor $e^{-M_H r}$.

Table 1 shows the effect of the Higgs term for various potentials,[30] Higgs masses, and VEV ratios, where we have taken $m_t = 50$ GeV. The Higgs can have striking effects; note, however, the similarity of the Cornell potential without a Higgs term to the Richardson potential with such a term. We have illustrated this problem by picking potentials that are not as physically well motivated as the Richardson potential. We would get similar, though less striking, effects by considering a QCD-inspired potential where one is free to vary $\Lambda_{\overline{MS}}$.

Figure 22 shows R($e^+e^- \rightarrow \mu^+\mu^-$), for toponium interfering with the Z, smeared with a beam width of 40 MeV, and $m_t = 47.5$ GeV. Note the qualitative similarity between the second and third figures.

Potential	M_H	ξ/η	$\langle r\rangle_{1S}$	$E_{2s}-E_{1s}$	$E_{2s}-E_{1p}$	$\Psi(0)_{1s}$	$\Psi(0)_{2s}/\Psi(0)_{1s}$
Richardson	—	0	.24	.999	.102	8.5	.52
	5	7	.18	1.58	.061	15.1	.42
	10	11	.133	2.37	−.037	26.4	.306
	20	10	.18	1.41	.016	18.0	.41
	40	8.2	.224	1.071	.08	11.4	.49
Cornell	—	0	.144	2.226	.015	23.3	.372
	10	4	.133	2.51	−.005	26.4	.354
Martin	—	0	.419	.455	.127	2.72	.75

Table 1. Calculated parameters of toponium (all units GeV to appropriate powers).

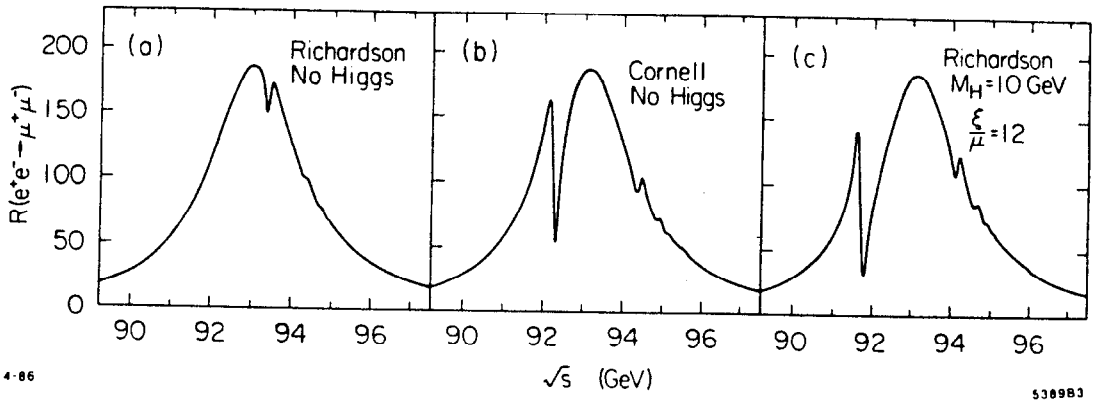

Figure 22. Effects of varying quarkonium potential.

REFERENCES

1. F. M. Renard, Z. Phys. **C1**, 225 (1979).

2. L. M. Sehgal and P. M. Zerwas, Nucl. Phys. **B183**, 417 (1981). See also R. Budny, Phys. Rev. **D20**, 2763 (1979), and J. D. Jackson, S.L. Olsen, and S.H.H. Tye, in *Proceedings of the 1982 Summer Study on Elementary Particles and Fields, Snowmass*, edited by R. Donaldson, R. Gustafson, and F. Paige (Amer. Inst. Phys., N.Y., 1983), p.175. L. M. Chang and J. N. Ng, TRIUMF preprint (1984) (unpublished).

3. W. Buchmüller, in *Cornell Z_0 Theory Workshop, Ithaca*, edited by M. E. Peskin and S.H.H. Tye (Cornell University, Ithaca, N.Y., 1982), p.210 and references therein; I. I. Y. Bigi and H. Krasemann, Z. Phys **C7**, 127 (1981); J. H. Kühn, in *Proceedings of the 1982 Schladming School (Electroweak Interactions), Schladming*, edited by H. Mitter (Springer-Verlag, Vienna, 1982), p.203; L. M. Sehgal, in *Proceedings of the 1983 Europhysics Study Conf. on Electroweak Effects at High Energies, Erice*, edited by H. D. Newman (Plenum, New York, 1985), (to be published); J. H. Kühn and S. Ono, Z. Phys. **C21**, 395 (1984); Erratum **C24**, 404 (1984); J. H. Kühn, Acta Phys. Pol. **B12**, 347 (1981).

4. E. Eichten, in *Proceedings of the 1984 SLAC Summer Institute on Particle Physics, Stanford*, edited by P. McDonough (Stanford Linear Accel. Center, Stanford, 1985), (to be published).

5. G. Arnison *et. al.*, Phys. Lett. **126B**, 398 (1983) and **135B**, 250 (1984); P. Bagnaia *et. al.*, Phys. Lett. **129B**, 130 (1983).

6. G. Arnison *et. al.*, Phys. Lett. **147B** 493 (1984).

7. P. J. Franzini and F. J. Gilman, Phys. Rev. **D32**, 237 (1985); S. Güsken, J. H. Kühn, and P. M. Zerwas, Nucl. Phys. **B262**, 393 (1985); J. H. Kühn, and P. M. Zerwas, Phys. Lett. **154B**, 448 (1985); L. J. Hall, S. F. King, and S. R. Sharpe, Nucl. Phys. **B260**, 510 (1985).

8. J. L. Richardson, Phys. Lett. **82B**, 272 (1979).

9. S. Coleman and H.J. Schnitzer, Phys. Rev. **134**, 863 (1964).

10. F. M. Renard, Springer Tracts in Mod. Phys. **63**, 98 (1972); Y. Dothan and D. Horn, Nucl. Phys. **B114**, 400 (1976).

11. Particle Data Group, Rev. Mod. Phys. **56**, No. 2, Part II, S296 (1984).

12. We take M_Z=93 GeV for the remainder of the thesis. All other masses are given relative to it, so that as a more exact value of the Z mass is measured, all our curves can be shifted appropriately. In addition we use $\sin^2\theta_W = 0.22$ and $\Gamma_Z = 2.7$ GeV (this does not include a contribution from the t quark); these values include the second order electroweak corrections.

13. The t and $\bar{t}$ quarks in the $^3S_1$ toponium states have a total width of $\approx$70 KeV to decay weakly for m_t=45 GeV, which is comparable to, or greater than, the combined width for such a state to decay by annihilation through photons or gluons, or to decay by a transition to another toponium state. Hence we take $\Gamma_{V_0} = 100$ KeV for illustrative purpose.

14. K. Gottfried, in *Proceedings of the 1981 International School of Nuclear Physics, Erice*, edited by D. Wilkinson (Pergamon Press, Oxford, 1982), p. 49. See also K. Gottfried, in *Proceedings of the Int. Europhysics Conf. on*

High Energy Physics (Proceedings of HEP83), Brighton, edited by J. Guy and C. Costain (Rutherford Lab., Chilton, 1983), p. 747.

15. We note that our levels, for the 1S, 2S, 3S, 1P and 2P states, agree with those presented by J. H. Kühn and S. Ono, Z. Phys. **C21**, 295 (1984); see also W. Buchmüller, in *Cornell Z_0 Theory Workshop, Ithaca*, edited by M. E. Peskin and S. H .H. Tye (Cornell University, Ithaca, N.Y., 1982), p.210.

16. R. Van Royen and V. Weisskopf, Nuovo Cimento, **50**, 617 (1967).

17. We have omitted QCD radiative corrections to Γ_{ee}; these would decrease the width by a factor of about 0.8.

18. E. Eichten and K. Gottfried, Phys. Lett. **66B**, 286 (1977). See also C. Quigg and J. L. Rosner, Phys. Lett. **72B**, 462 (1978).

19. J. Lee-Franzini, in *Proceedings of the 22nd Int. Conf. on High Energy Physics, Leipzig, 1984*, edited by A. Meyer and E. Wieczorek (Akademie der Wissenschaften der DDR, Zeuthen, 1985), p. 150. See also K. Han *et. al.*, Phys. Rev. Lett. **55**, 36 (1985).

20. R. Stiening, private communication.

21. We thank P. Zerwas for pointing out the still sizable effects in asymmetries left after smearing when toponium is well below the Z. See Ref. 7 for a detailed discussion.

22. A. Martin, CERN preprint TH4060/84 (1984) (lectures given at Int. School of Subnuclear Physics, Erice, Italy, Aug 5-15, 1984).

23. L. Susskind, Phys. Rev. **D20**, 2619 (1979); E. Farhi and L. Susskind, Phys. Rept. **74**, 277 (1981), and references therein.

24. S. Glashow and S. Weinberg, Phys. Rev. **D15**, 1958 (1977), E. A. Paschos, Phys. Rev. **D15**, 1966 (1977).

25. H. E. Haber, G. L. Kane and T. Sterling, Nucl. Phys. **B161**, 493 (1979).

26. L. F. Abbott, P. Sikivie and M. B. Wise, Phys. Rev. **D21**, 1393 (1980).

27. G. G. Athanasiu and F. J. Gilman, Phys. Lett. **153B**, 274 (1985).

28. G. G. Athanasiu, P. J. Franzini and F. J. Gilman, Phys. Rev. **D32**, 3010 (1985). See this reference for a detailed discussion and further references.

29. A. Martin, Nucl. Phys. **B254**, 528 (1985).

30. J. L. Richardson, Phys. Lett. **82B**, 272 (1979); E. Eichten *et al.*, Phys. Rev. **D17**, 3090 (1979); **D21**, 203 (1980) (referred to as "Cornell" model); A. Martin, Phys. Lett. **93B**, 338 (1980).

PART II

PHENOMENOLOGY OF AN EXTRA Z^0 IN e^+e^- COLLISIONS*

1. Introduction

Many extensions of the standard model, such as grand unified theories and left-right symmetric models, propose a gauge sector of greater symmetry than the $SU(3) \times SU(2) \times U(1)$ of the standard model. The recent advent of superstring theories[1] has given a further boost to interest in this possibility, since the combined low energy gauge group will generally be larger than $SU(3)_C \times SU(2)_L \times U(1)_Y$ in these theories.[2,3] More particularly, superstrings have revived interest in grand unified theories based on the exceptional groups, especially E_6. From the experimental side, the prospect of having electron-positron colliders operating near 100 GeV center-of-mass energies in the near future has made it imperative to explore what "new physics" we might look for. The presence of additional neutral gauge bosons may well be one of the "easier" varieties of physics beyond the standard model to detect.

Most attention has been concentrated on the phenomenological implications of one additional abelian factor in the low energy electroweak gauge group. This not only is the simplest sort of generic extension of the standard model, but was an early favorite arising from superstrings. It is by no means the only possibility[3,4] even within the framework of early scenarios for the derivation of

* This work has previously been discussed in P. J. Franzini and F. J. Gilman, to be published in Phys. Rev. **D** (1986).

the effective low energy theory from the theory at the Planck scale. We shall concentrate on this case here, mainly for simplicity and definiteness.

The new extra neutral gauge boson, Z', will generally mix with the Z of the standard model. The resulting physical states then will be linear combinations of the initial Z and Z'. In particular, the physical Z will have an altered mass and couplings compared to expectations based upon the standard model.

The constraints that the measured versus expected Z mass, the neutral current data, and the Higgs structure (and therefore structure of the $Z - Z'$ mass matrix) of superstring inspired models impose on the Z' mass and its mixing with the Z have been examined in a number of previous works.[5-8] In various combinations in different papers, these constraints have been used to limit the allowed domain of Z' parameters in specific models. There has also been (both previous to and concurrent with superstrings) much study of the effects of a Z' upon electron-positron annihilation cross sections and asymmetries.[9-17] Some of the work on electron-positron annihilation has been done without considering the constraints[5-8] already pre-existing from other experimental information. In this part of the thesis we first review these constraints as they presently limit the range of phenomenological possibilities. We also show the further restrictions on the Z' parameters which may be possible in the future from accurate determinations of M_Z and M_W.

We then examine what can be learned from the magnitude of the cross section for annihilation into lepton and quark pairs at the Z peak. With the concentration on sophisticated experiments, it has been overlooked by many authors that this simple information, available at a relatively early stage of experimentation

at the Z peak, will already further limit the range of allowed Z' masses and mixing angles in a significant way. With this as background, we then consider what can be learned with polarized beams at and above the Z peak. Here we make no claim to uniqueness, as in one theory or another much of this work has also been done by others.[9-13,15-17] However, we put the knowledge to be gained with polarized beams into the same format of Z' mass and mixing angle, and so put this in the proper perspective of what is already known from other experiments.

Chapter 2 of this part deals with the models under consideration: the respective electroweak couplings of the Z and Z', their mass matrix, and corresponding mixing. Chapter 3 treats the existing limits on such models. Chapter 4 begins with a treatment of what can be learned by electron-positron annihilation measurements at the Z peak without having polarized beams. The further restrictions that can be made using polarized beams follow at the end of that chapter. Finally, in Chapter 5 we examine the possibilities of learning additional information, particularly in the case where there is little or no mixing between the Z and Z', by doing experiments in the energy region above the Z. The combination of all these measurements is found to provide a very sensitive indication of new gauge bosons up to energies of several hundred GeV.

2. Preliminaries

Superstring theories favor (but do not require) a high energy gauge group $E_8 \times E_8'$, in ten-dimensional spacetime.[18] The second E_8 describes the so-called "shadow world," which may trigger supersymmetry breaking, but interacts with ordinary matter only gravitationally, and shall be ignored here. Six of the ten spacetime dimensions must be compactified, with a radius smaller than 10^{-30}cm, characteristic of the Planck (or unification) scale. The interest in preserving $N = 1$ supersymmetry in the low-energy limit of the theory has focussed attention on six-dimensional manifolds with $SU(3)$ structure (manifolds with $SO(6)$ structure might also be relevant).[2] The "low"-energy gauge group will therefore consist of those transformations of E_8 commuting with $SU(3)$ (or $SO(6)$). Hence we need to find the maximal subalgebras of E_8 with $SU(3)$ (or $SO(6)$) factors. E_8 can be described in terms of the following diagram.

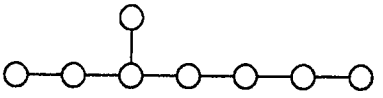

Figure 23. Dynkin diagram for E_8.

Each dot of this diagram represents a simple root vector of E_8. A root vector is defined as follows: let $\{H_i\}(i = 1, \cdots, r)$ be a maximal set of simultaneously diagonalizable generators of the Lie algebra (this set is known as the *Cartan subalgebra*; r equals the rank of the algebra). If we write the remaining generators

as $E_{\vec{\alpha}}$, we have the commutation relations

$$[H_i, E_{\vec{\alpha}}] = \alpha_i E_{\vec{\alpha}} \tag{2.1}$$

where $\vec{\alpha}$ is an r-component vector called a *root vector*, and the generators are labeled by their root vectors. A *positive* root vector is one with first nonzero component (in some given basis and ordering scheme) positive. And a *simple* root is one that cannot be expressed as a sum of two positive roots. All roots can be generated from the simple roots. The number of simple roots equals the rank of the group (the simple roots form a basis for the root vectors). The dots representing roots are connected by a single line if the angle between the roots is $2\pi/3$; they are unconnected if the roots are orthogonal (there are two other possibilities, which we shall not go into). Thus, for example, consider $SU(3)$. If we work in terms of the λ matrices of Gell-Mann* we can take the diagonal matrices λ_3 and λ_8 as forming the Cartan subalgebra. It is more convenient to work with the combinations

$$T_\pm = \frac{\lambda_1 \pm i\lambda_2}{2},\ T_z = \frac{1}{2}\lambda_3,\ V_\pm = \frac{\lambda_4 \pm i\lambda_5}{2},\ U_\pm = \frac{\lambda_6 \pm i\lambda_7}{2},\ Y = \frac{1}{\sqrt{3}}\lambda_8. \tag{2.2}$$

We find then that

⋆ See, for example, Ref. 19 for the explicit form of these matrices, and an excellent introduction to Lie algebras; see also Ref. 20 for discussions and many useful tables.

$$
\begin{aligned}
&[T_+, T_z] = -T_+,\ [T_+, Y] = 0 \text{ giving } \vec{\alpha}_1 = (-1, 0) \\
&[T_-, T_z] = T_-,\ [T_-, Y] = 0 \text{ giving } \vec{\alpha}_2 = (1, 0) \\
&[U_+, T_z] = \frac{1}{2}U_+,\ [U_+, Y] = -U_+ \text{ giving } \vec{\alpha}_3 = (.5, -1) \\
&[U_-, T_z] = -\frac{1}{2}U_-,\ [U_-, Y] = U_- \text{ giving } \vec{\alpha}_4 = (-.5, 1) \\
&[V_+, T_z] = -\frac{1}{2}V_+,\ [V_+, Y] = -V_+ \text{ giving } \vec{\alpha}_5 = (-.5, -1) \\
&[V_-, T_z] = \frac{1}{2}V_-,\ [V_-, Y] = V_- \text{ giving } \vec{\alpha}_6 = (.5, 1)
\end{aligned}
\tag{2.3}
$$

So the positive roots, in this basis, are $\vec{\alpha}_2$, $\vec{\alpha}_3$ and $\vec{\alpha}_6$, and the simple roots are $\vec{\alpha}_3$ and $\vec{\alpha}_6$, giving the Dynkin diagram in Figure 24.

Figure 24. Dynkin diagram for $SU(3)$.

The linear independence and other requirements on simple roots can be expressed in terms of a simple set of rules on the diagrams that allow us to determine the set of *all* allowed Lie algebras. These consist of the four sequences of classical Lie algebras: $SU(N+1)$, $SO(2N)$, $Sp(2N)$ and $SO(2N+1)$, also known as A_N, D_N, C_N, and B_N, and the five additional exceptional Lie algebras: G_2, F_4, E_6, E_7, and E_8. In Fig. 25, we show the Dynkin diagrams for some of these algebras.

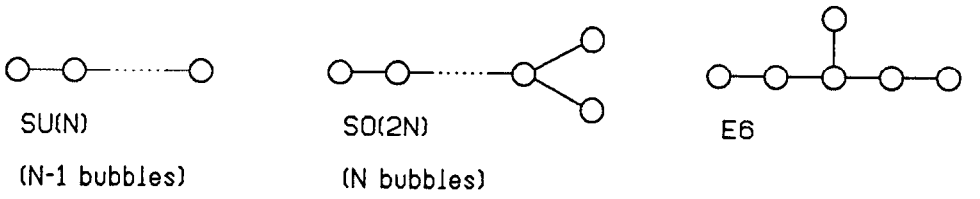

Figure 25. Dynkin diagrams for $SU(N)$, $SO(2N)$, and E_6.

Subalgebras can be found diagrammatically in the following ways. The regular subalgebras (there are a few other, non-regular ones, which we will not worry about) fall into two classes: nonsemisimple (i.e., containing a $U(1)$ factor) and semisimple (i.e., a product of one or more simple, or non-abelian, factors). Each maximal nonsemisimple subalgebra is just a $U(1)$ factor times a semisimple factor given by the Dynkin diagram for the original algebra minus any one dot. The maximal semisimple subalgebras are obtained by removing one dot from the "extended" Dynkin diagram. This diagram is found by constructing a set of roots that satisfies all the requirements of a simple root system, except linear independence. It turns out that only one root can be added, and it is unique. The extended diagram for E_8 is shown in Figure 26.

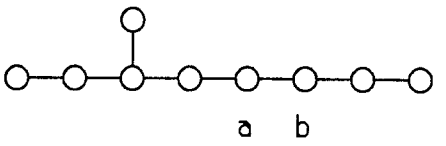

Figure 26. Extended diagram for E_8.

We see then, removing the dot labeled b, that for compactification on a six

dimensional manifold with $SU(3)$ holonomy, the remaining symmetry is E_6; for $SO(6)$ (removing the dot labeled a), we get $SO(10)$. We shall only consider the former case. Removing two more dots from the E_6 diagram, we find the breaking pattern

$$E_6 \rightarrow SO(10) \times U(1)_\psi \tag{2.4}$$

and then,

$$SO(10) \rightarrow SU(5) \times U(1)_\chi, \tag{2.5}$$

where we have labelled the $U(1)$'s in a now standard manner.[21] If the $SU(5)$ contains the standard $SU(3)_C \times SU(2)_L \times U(1)_Y$, then any extra $U(1)$ from the breaking of E_6 must be a combination of $U(1)_\psi$ and $U(1)_\chi$. The corresponding Z' will be a combination of Z_ψ and Z_χ which is defined by

$$Z'(\theta_{E_6}) = Z_\psi \cos\theta_{E_6} + Z_\chi \sin\theta_{E_6}. \tag{2.6}$$

In the particular case of superstring theories broken by Wilson loops to a rank 5 group, a special $Z(\theta_{E_6})$ is specified:

$$Z_\eta = -\sqrt{5/8}\ Z_\psi + \sqrt{3/8}\ Z_\chi. \tag{2.7}$$

It is this Z_η that we shall be considering primarily in this part of the thesis, but we shall at various places consider what would happen to the quantity under discussion if the Z' were Z_ψ or Z_χ, as well as other intermediate possibilities.

The Lagrangian describing the interaction of the neutral gauge bosons of an electroweak theory containing a Z' with the corresponding currents can be written as:

$$\mathcal{L}_{NC} = eA_\mu J^\mu_{em} + g_z Z_\mu J^\mu_Z + g' Z'_\mu J^\mu_{Z'} \tag{2.8}$$

where the couplings are given by

$$g_z = \frac{e}{\sqrt{x_W - x_W^2}} \qquad \text{and} \qquad g' = \frac{e}{\sqrt{1 - x_W}} \quad . \tag{2.9}$$

Here J^μ_{em} is the electromagnetic current, and $J^\mu_Z = J^\mu_{3L} - x_W Q^\mu$ is the standard $Z-$boson current; we define* $J^\mu_{Z'} = \bar{f}_L \gamma^\mu \widetilde{Q}_L f_L + \bar{f}_R \gamma^\mu \widetilde{Q}_R f_R$ (the charge $\widetilde{Q}$ is a number dictated by the group structure), and $x_W = \sin^2\theta_W$.

The couplings of Z_ψ, Z_χ, and therefore Z_η follow from pure group theory and are given[22] in Table 2. We specify not only the couplings to the known fermions which comprise the 10 plus $\bar{5}$ representations of $SU(5)$, but to the "exotic" fermions which make up the full 27 dimensional representation of E_6. The D is a charge $-e/3$ quark; the N an $SU(2)_L$ singlet, neutral lepton; and the E_0, E^- an $SU(2)_L$ doublet of leptons. The coupling is related to the charge by a factor of $\sqrt{5/3}(e/\cos\theta_W)$. Note that because of the breaking pattern in Eqs. (2.4) and (2.5), any $Z'(\theta_{E_6})$ has the same coupling to each member of a given $SU(5)$ multiplet. The Z has different couplings generally to different members of an $SU(5)$ multiplet, but since it couples like a generator (or more exactly,

---

* We would like to thank W. J. Marciano for pointing out a factor of two error in the expression for this current.

$SO(10)$	$SU(5)$	$2\sqrt{10}Q_\chi$	$\sqrt{24}Q_\psi$	$2\sqrt{15}Q_\eta$
16	$10(u, d, \bar{u}, e^+)$	-1	1	-2
	$\bar{5}(\bar{d}, \nu, e^-)$	3	1	1
	$1(\bar{N})$	-5	1	-5
10	$5(D, \bar{E}^0, E^+)$	2	-2	4
	$\bar{5}(\bar{D}, E^0, E^-)$	-2	-2	1
1	$1(S^0)$	0	4	-5

Table 2. Charges of the fermions in the 27 dimensional representation of E_6 (from Ref. 7).

	$\Gamma(Z' \to \text{all})$	$BR(e^+e^-)$	$BR(u\bar{u})$	$BR(d\bar{d})$
ψ	4.9 (23.)	4.4% (.93%)	13% (2.8%)	13% (2.8%)
χ	11 (23.)	6.1% (2.8%)	3.6% (1.7%)	18% (8.3%)
η	5.8 (23.)	3.7% (.93%)	18% (4.4%)	11% (2.8%)

Table 3. Total widths and branching ratios of the Z_χ, Z_ψ, and Z_η to fermion pairs.

a linear combination of generators), the sum over an $SU(5)$ multiplet of the Z charges vanishes. Therefore,

$$\sum_{SU(5)\ multiplet} Q_Z Q_{Z'(\theta_{E_6})} = 0. \tag{2.10}$$

The width of the Z' is now determined. In Table 3 we give the total widths in units of $10^{-3}M_{Z'}$ and the branching ratios for decays into $u\bar{u}$, $d\bar{d}$, and e^+e^-, for each case considering the possibility that none or all (in parentheses) of the "exotic" fermions are light enough to be decay products of the Z'.

The physical Z and Z' bosons will not be the states which we have been

discussing till now, but a linear combination, since an extra neutral gauge boson will generally mix with the Z of the standard model. The two channel mass matrix has the form

$$M^2 = \begin{pmatrix} M_{Z_0}^2 - iM_{Z_0}\Gamma_{Z_0} & \delta M^2 \\ \delta M^2 & M_{Z_0'}^2 - iM_{Z_0'}\Gamma_{Z_0'} \end{pmatrix} \tag{2.11}$$

and for δM^2 small will be diagonalized by a rotation through an angle

$$\theta_{MIX} \approx \frac{\delta M^2}{M_{Z'}^2 - M_Z^2}. \tag{2.12}$$

The amplitude for e^+e^- annihilating to a $f\bar{f}$ final state is then

$$\mathcal{A}_{IJ} = \begin{pmatrix} g_{Z_0} & g_{Z_0'} \end{pmatrix}_{f_J} \begin{pmatrix} s - M_{Z_0}^2 + iM_{Z_0}\Gamma_{Z_0} & \delta M^2 \\ \delta M^2 & s - M_{Z_0'}^2 + iM_{Z_0'}\Gamma_{Z_0'} \end{pmatrix}^{-1} \begin{pmatrix} g_{Z_0} \\ g_{Z_0'} \end{pmatrix}_{e_I} + \mathcal{A}_\gamma. \tag{2.13}$$

We diagonalize the mass matrix to find the physical Z mass, which will be shifted downward from its "bare", standard model value, just as the Z' will be shifted upward (by an equal and opposite amount in the square of the mass):

$$\Delta M_Z \approx \frac{M_Z^2 - M_{Z'}^2}{2M_Z}\,\theta_{MIX}^2. \tag{2.14}$$

In a given theory, the Higgs content gives restrictions on the elements of the mass matrix in Eq. (2.11). These restrictions have been formulated in the general case by Cvetič and Lynn.[13] In the particular case of Z_η, the Z and Z' masses are generated by two Higgs doublets—H and H', and one Higgs singlet—N. These particles have vacuum expectation values (VEV) v_1, v_2 and χ, respectively. The

charges of these particles are H—$(1, \frac{4}{3})$, H'—$(-1, \frac{1}{3})$, and N—$(0, -\frac{5}{3})$ where we have given the Z charge, then the Z'. Recalling that $g'/g_Z = \sqrt{x_W}$, we have

$$M^2 = M_{Z_0}^2 \begin{pmatrix} 1 & \sqrt{x_W}\,\dfrac{4v_1^2 - v_2^2}{3(v_1^2+v_2^2)} \\ \sqrt{x_W}\,\dfrac{4v_1^2 - v_2^2}{3(v_1^2+v_2^2)} & x_W\,\dfrac{16v_1^2 + v_2^2 + 25\chi^2}{9(v_1^2+v_2^2)} \end{pmatrix}, \tag{2.15}$$

using $M^2 = \sum Q_i^2 v_i^2$. The off diagonal element of this matrix can range from $-\frac{1}{3}\sqrt{x_W}$ to $\frac{4}{3}\sqrt{x_W}$, while $M_{Z'}$ is essentially free to vary independently. Thus we have the following bound on the mixing angle:

$$\frac{-\frac{8}{3}\sqrt{x_W}}{\frac{M_{Z'}^2}{M_Z^2} - 1} < \tan 2\theta < \frac{\frac{2}{3}\sqrt{x_W}}{\frac{M_{Z'}^2}{M_Z^2} - 1}. \tag{2.16}$$

The charges of the physical Z are therefore changed from those of the standard model through the rotation that diagonalizes the mass matrix in Eq.(2.11):

$$g_{Z_{physical}} = g_Z \cos\theta_{MIX} - g_{Z'(\theta_{E_6})} \sin\theta_{MIX}. \tag{2.17}$$

The partial widths of the Z, given by $\Gamma_Z \propto g_Z^2 M_Z$, are correspondingly altered, with changes which are linear in θ_{MIX} for small mixing.

We can also find the physical widths in a manner analogous to that used to obtain the masses, by diagonalizing the mass matrix and extracting the width by looking at its imaginary part. Diagonalizing the mass matrix in Eq. (2.11), we find

$$M_Z^2 - iM_Z\Gamma_Z \approx \frac{M_{Z_0}^2 - iM_{Z_0}\Gamma_{Z_0} - \theta^2(M_{Z_0'}^2 - iM_{Z_0'}\Gamma_{Z_0'})}{1-\theta^2} \tag{2.18}$$

giving

$$M_Z\Gamma_Z - M_{Z_0}\Gamma_{Z_0} \approx (M_{Z_0}\Gamma_{Z_0} - M_{Z_0'}\Gamma_{Z_0'})\theta_R^2 - 2(M_{Z_0}^2 - M_{Z_0'}^2)\theta_R\theta_I \qquad (2.19)$$

where

$$\theta = \theta_R + i\theta_I \approx \frac{\delta M^2}{M_{Z_0'}^2 - M_{Z_0}^2 - (iM_{Z_0'}\Gamma_{Z_0'} - iM_{Z_0}\Gamma_{Z_0})}. \qquad (2.20)$$

From this expression for θ we see that

$$\theta_R^2(M_{Z_0}\Gamma_{Z_0} - M_{Z_0'}\Gamma_{Z_0'}) \sim \theta_R\theta_I(M_{Z_0}^2 - M_{Z_0'}^2) \qquad (2.21)$$

and therefore that the shift in Γ_Z is $\mathcal{O}(\Gamma\theta_R^2)$.

The error in this approach lies in two omissions. First, we must include an imaginary off-diagonal term proportional to $ig_{Z_0}g_{Z_0'}M_{Z_0}M_{Z_0'}$, analogous to the terms $iM_{Z_0}\Gamma_{Z_0} \propto ig_{Z_0}^2M_{Z_0}^2$, and $iM_{Z_0'}\Gamma_{Z_0'} \propto ig_{Z_0'}^2M_{Z_0'}^2$. Moreover, since the masses M_{Z_0} and $M_{Z_0'}$ are far apart, we cannot neglect the energy-dependence of the widths. Since we are working in the vicinity of the Z_0, we replace $M_{Z_0'}$ by M_{Z_0} in the expressions $ig_{Z_0'}^2M_{Z_0'}^2$ and $ig_{Z_0}g_{Z_0'}M_{Z_0}M_{Z_0'}$. The corrected mass matrix is

$$\begin{pmatrix} M_{Z_0}^2 - iM_{Z_0}\Gamma_{Z_0} & \delta M^2 - iM_{Z_0}\sqrt{\Gamma_{Z_0}\Gamma_{Z_0'}\frac{M_{Z_0}}{M_{Z_0'}}} \\ \delta M^2 - iM_{Z_0}\sqrt{\Gamma_{Z_0}\Gamma_{Z_0'}\frac{M_{Z_0}}{M_{Z_0'}}} & M_{Z_0'}^2 - iM_{Z_0}\frac{M_{Z_0}}{M_{Z_0'}}\Gamma_{Z_0'} \end{pmatrix}. \qquad (2.22)$$

We now have an equation similar to Eq. (2.19):

$$M_Z\Gamma_Z - M_{Z_0}\Gamma_{Z_0} \approx (M_{Z_0}\Gamma_{Z_0} - M_{Z_0'}\left(\frac{M_{Z_0}^2}{M_{Z_0'}^2}\right)\Gamma_{Z_0'})\theta_R^2 - 2(M_{Z_0}^2 - M_{Z_0'}^2)\theta_R\theta_I \quad (2.23)$$

but θ is given by

$$\theta \approx \frac{\delta M^2 - iM_{Z_0}\sqrt{\Gamma_{Z_0}\Gamma_{Z_0'}\frac{M_{Z_0}}{M_{Z_0'}}}}{M_{Z_0}^2 - M_{Z_0'}^2 - iM_{Z_0}\Gamma_{Z_0} + iM_{Z_0'}\Gamma_{Z_0'}} \tag{2.24}$$

so that

$$\theta_I \approx \frac{(M_{Z_0'}\Gamma_{Z_0'} - M_{Z_0}\Gamma_{Z_0})\delta M^2 + (M_{Z_0}^2 - M_{Z_0'}^2)M_{Z_0}\sqrt{\Gamma_{Z_0}\Gamma_{Z_0'}\frac{M_{Z_0}}{M_{Z_0'}}}}{(M_{Z_0}^2 - M_{Z_0'}^2)^2}. \tag{2.25}$$

Because of this new second term in Eq. (2.25), θ_I is $O(\Gamma/M)$; therefore the second term in Eq. (2.23) gives a contribution to $\Delta\Gamma$ of $O(\Gamma\theta_R)$. This method can be shown to give the same answer as the rotated coupling method.

In part I of this thesis, we did not encounter this subtlety, since the equivalent of $g_{Z_0'}$, namely, $g_{t\bar{t}_0}$, is very close to zero; moreover, the $t\bar{t}_0$ mass is near that of the Z_0; hence we need not consider the energy-dependence of the widths. The more naive diagonalization approach is then a valid approximation, and the rotated coupling method gives the same $O(\theta^2)$ result, since the θ dependence now comes in only in $g_{Z_0}\cos\theta$.

Although present in the partial widths, the term linear in θ_{MIX} in the total width of the Z vanishes, since it involves a sum over $Q_Z Q_{Z'(\theta_{E_6})}$ and (see Eq. (2.10)) this sum is zero when taken over all members of an $SU(5)$ multiplet. The known quarks and leptons in each generation completely fill two such multiplets, and the other "exotic" fermions of the 27 of E_6 fill other $SU(5)$ multiplets. So, with or without the full set of exotic decays, the change in the total width of the Z is quadratic rather than linear in θ_{MIX} for small mixing. Therefore, $\Delta\Gamma/\Gamma$ is

of the same order as $\Delta M/M$. However, experimentally, we expect the *absolute* errors on Γ_Z and M_Z to be comparable, so the measurement of total Z width does not promise to be useful to us.

3. Current Limits

The constraints which the measured as compared to expected (in the standard model) Z mass, the neutral current data, and the Higgs content of superstring models impose have been examined separately or in combination in a number of papers.[5-8] They serve to limit the values of the Z' mass and mixing angle and it is useful to briefly review them, if only to see what remains for e^+e^- colliders to do.

We concentrate on Z_η. For the constraint provided by the measured mass of the Z, we have taken a combination of the present statistical and systematic errors as indicating agreement with theory to within 3 GeV and plotted it as the dash-dot curve in Figure 27.* We compare these limits with those found by Durkin and Langacker[7] from neutral current data; their boundary of the allowed region is plotted as the dashed curve.[24] The solid curve represents the bound obtained from the Higgs structure of the mass matrix. As shown in Figure 27, the mixing angles allowed for a Z' which has unmixed gauge couplings corresponding to Z_η obey $|\theta_{MIX}| \lesssim 0.1$ and the region of allowed masses starts at about 130 GeV. These constraints cover the same general area; for Z' masses up to several times the Z mass, it is the neutral current data and/or the limit on the shift

* We compare the measured value of M_Z with its value as calculated from the measured value of M_W, using $M_W = 38.65/\sin\theta_W$ (at the one-loop level) to fix $\sin\theta_W$. The UA1 experiment measures M_Z to be 1 GeV smaller than this "theoretical" value determined from M_W. Thus, taking the statistical errors of $M_Z(th)$ and $M_Z(exp)$ in quadrature, and ignoring the systematic errors (which come from an energy scale uncertainty which should affect both numbers approximately equally) we find that a 3 GeV decrease in M_Z from $M_Z(th)$ is about a 1.1σ effect. UA2, however, measures M_W to be smaller; $M_Z(th)$ is slightly smaller than $M_Z(exp)$, and a 3 GeV decrease from $M_Z(th)$ is a 2σ effect. We use numbers from Ref. 23. (It is amusing to note that using previous (1984) data these numbers would become 3σ for UA1 and 1σ for UA2).

of the Z mass which provide more stringent constraints than the Higgs content. The surprisingly low mass value allowed for the Z' is due to the small (compared to the Z) couplings to ordinary fermions of the Z_η.

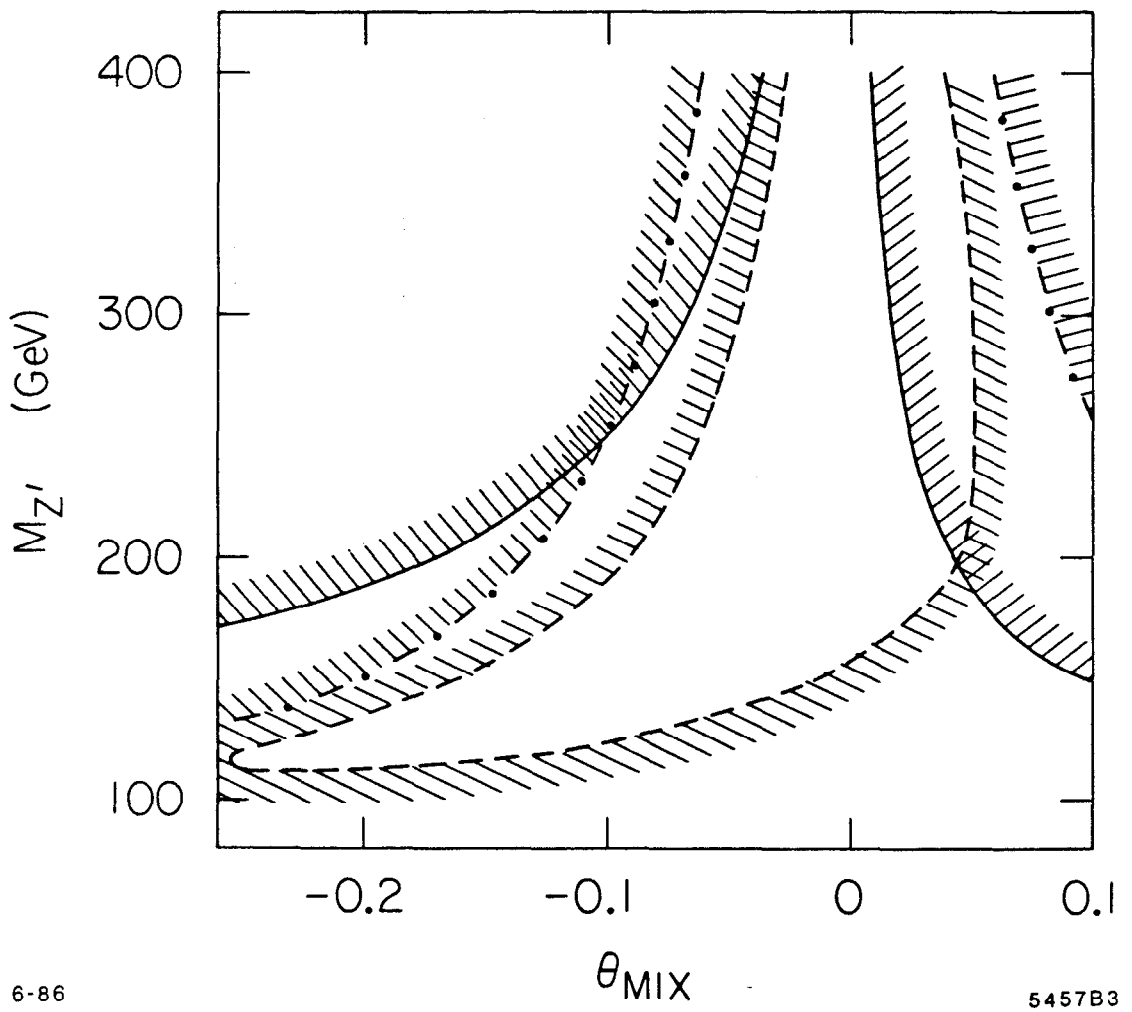

Figure 27. Current constraints on the mass and mixing angle of a possible Z_η.

In the following we take the inner (allowed) region from Figure 27 and use it as a reference curve for the bounds obtainable from future experiments (plotted as a dotted line). For example, in Figure 28 we show the bounds from measuring the Z mass (relative to the W) with an error of 500 MeV (curve 1) and of 64

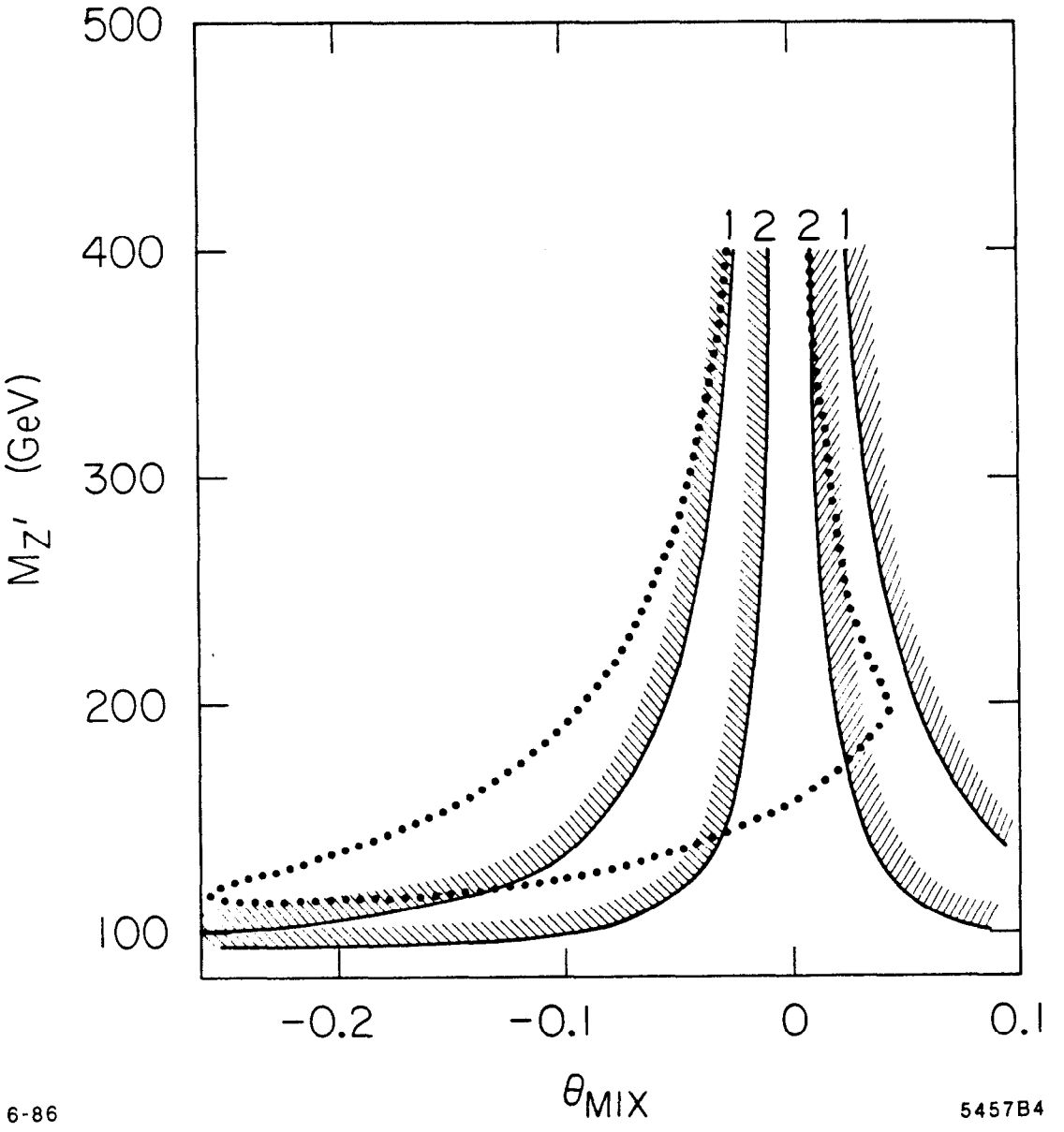

Figure 28. Constraints on Z''s from future measurements of M_Z and M_W.

MeV (curve 2). We regard the former as probably attainable early in the next generation of hadron collider experiments and the latter as a possible ultimate accuracy.† Particularly in the latter case the region of parameter space allowed

† The value of 64 MeV is obtained by combining in quadrature an error on the "theoretical" value of M_Z of 61 MeV (from an optimistic future error on the measured value of M_W of

for the Z' is diminished considerably. Note that these limits are relevant to the case where there are only additional Z''s. If there are additional W''s as well, they generally mix with the W, adding additional parameters, and removing the connection between the observed W mass and the unmixed Z mass.

75 MeV) with an optimistic error on the experimental value of M_Z measured at LEP of 20 MeV.

4. Limits from Measurements at the Z Peak

With the results of the last chapter as background, we now direct our attention to electron-positron annihilation at the peak of the Z. We begin with the most straightforward measurements: the shift in the mass and width of the Z and the cross section for production of fermion-antifermion pairs at the peak.

Using the equations given in Chapter 2, we calculate the results shown in Figure 29 for the change in the mass and total width of the Z, and the cross sections for various final-state fermion pairs in electron-positron annihilation at the (mixed) Z peak as a function of θ_{MIX} (when we are considering a Z_η). The mass shift was treated in Chapters 2 and 3; it depends on both the mass of the Z' and the mixing angle (we have taken $M_{Z'} = 200$ GeV). The other changes occur because of the altered couplings of the physical Z due to mixing with the Z'. Therefore they depend essentially only on the mixing angle with the Z as long as the Z' is many widths away from the Z.

The shift in the total width is very small, and is within anticipated measurement systematic errors. This is expected on the basis of Eq. (2.10) through cancellations of the first order terms in θ_{MIX} when the sum over modes includes all members of an $SU(5)$ multiplet.

This is not true for the cross section for individual fermion-antifermion final states which is proportional to the partial width of the Z into these particular channels and to $\Gamma_{e^+e^-}$. There are changes of roughly 10% for variations of θ_{MIX} by ± 0.1. Such a change should be significant, particularly for $e^+e^- \to Z \to e^+e^-$ (or equivalently, $e^+e^- \to Z \to \mu^+\mu^-$), where a 3% measurement of the cross

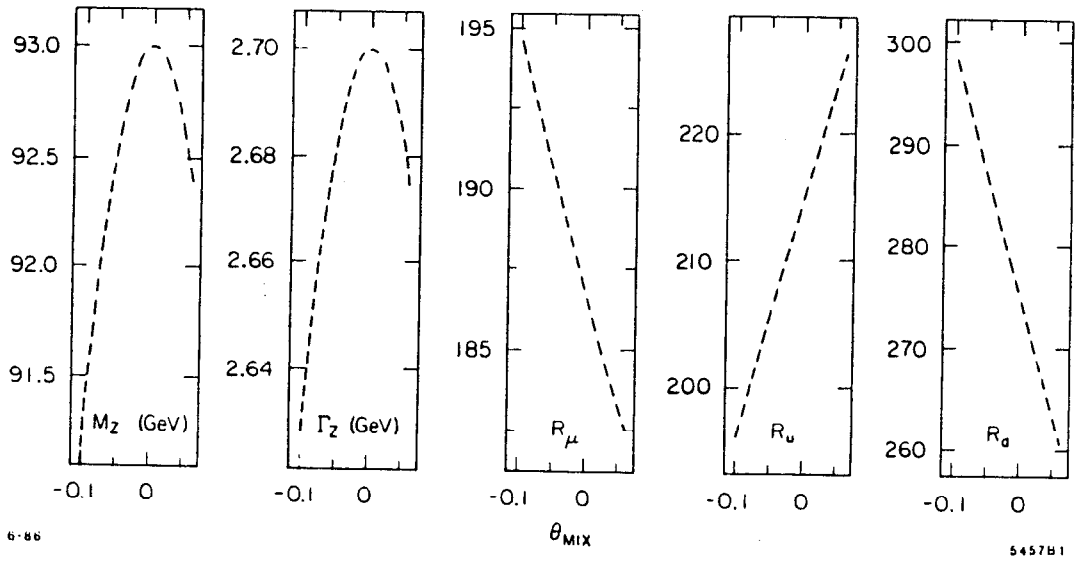

Figure 29. Change in M_Z, Γ_Z and R for $e^+e^- \rightarrow \mu^+\mu^-$,$u\bar{u}$ and $d\bar{d}$ from mixing with Z_η.

section seems possible.[25] This corresponds to a 1σ limit on θ_{MIX} of ± 0.08.

Quark-antiquark cross sections can be determined to poorer accuracy than that for mu pairs; 10% is probably a fair estimate[23] for $b\bar{b}$ (isolatable through semileptonic decays), which is the same as $d\bar{d}$ or $s\bar{s}$. The cross sections for $u\bar{u}$ and $c\bar{c}$ can then be obtained by subtraction from the total of all hadronic decays. Because of this decreased accuracy of measurement, the hadronic cross sections provide less of a constraint than the more accurately measured muon pair cross section, even though the change in the latter due to mixing with Z_η is smaller.

Note also that mixing with Z_η produces a characteristic pattern where the cross section for $\mu^+\mu^-$ and $d\bar{d}$ increases when that for $u\bar{u}$ decreases and *vice*

versa. The couplings of each $Z_{\theta_{E_6}}$ are different and produce recognizably different patterns.

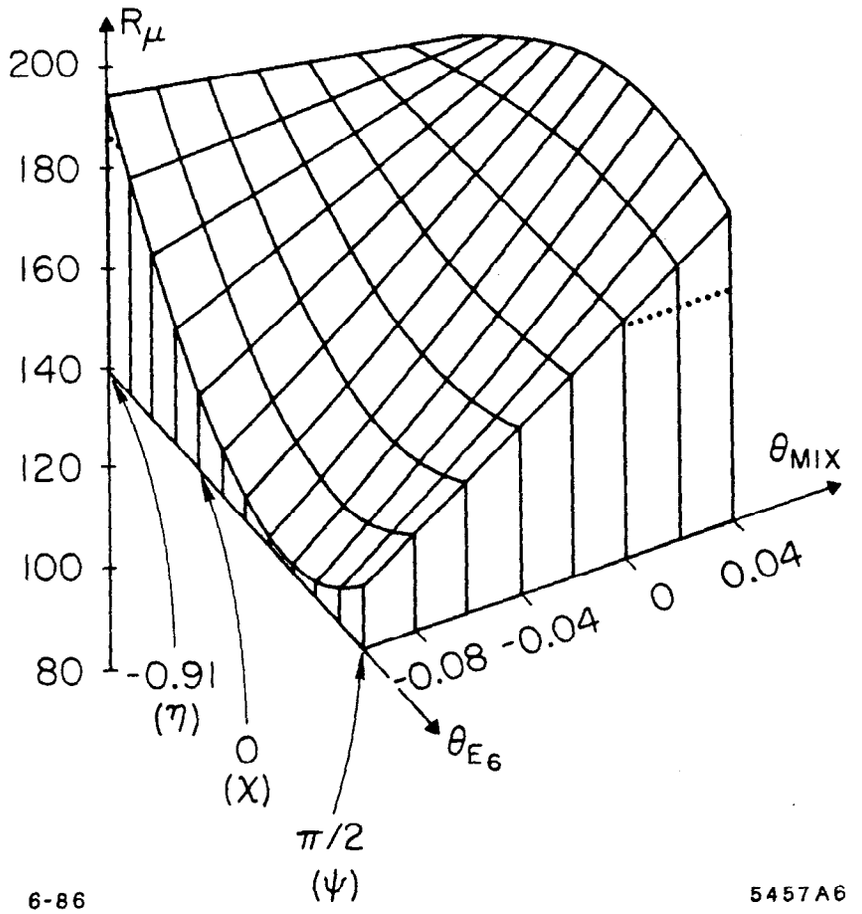

Figure 30. R_μ versus θ_{MIX} and θ_{E_6}. The dotted line gives R_μ when no Z' is present.

This is illustrated in a different way in Figure 30, where the cross section at the Z peak for annihilation into muon pairs is shown versus both θ_{MIX} and θ_{E_6}. Depending on which Z' is chosen, one gets an increased or decreased cross section from the value one would have with no Z' (shown by the dotted line). Note that the particular case of a Z_η gives a nearly minimal effect for this particular cross

section. Choosing instead Z_ψ or Z_χ for our Z' would have produced much greater effects in the muon pair cross section and correspondingly better limits on θ_{MIX}. For example, we would have obtained $|\theta_{MIX}| \lesssim 0.04$ if the Z' was taken as Z_ψ.

There is a small front-back asymmetry at the Z in the standard model. Mixing with a Z' alters its magnitude as has been calculated in detail elsewhere.[11-17] In Figure 31 we show the limits placed on $M_{Z'}$ and θ_{MIX} by future measurements at the Z peak of the front-back asymmetry in $e^+e^- \rightarrow \mu^+\mu^-$ (and their agreement within one sigma with the value expected in the standard model) with 10^4 (curve 1), 10^5 (curve 2), and and 10^6 (curve 3) measured Z's. The limits are almost independent of $M_{Z'}$; the slight bending of the curves bounding the allowed region for the lowest Z' masses is due to finite width effects of the Z' (calculated with decays into non-exotic fermions only).

This measurement is unlikely to add very much to the limits which will be available from other measurements in a similar time period. Measurements with quarks in the final state are difficult because of the small samples of potential events remaining after cuts to isolate a quark rather than an antiquark, and are complicated by $B - \bar{B}$ mixing.[26]

Finally we turn to the information that may be obtained when a longitudinally polarized electron beam is available. We can write the asymmetry

$$A_{POL} = \frac{\sigma_R - \sigma_L}{\sigma_R + \sigma_L} = \frac{2\, v_e\, a_e}{|v_e|^2 + |a_e|^2}, \tag{4.1}$$

where σ_R and σ_L are the cross sections for right- and left-handed incident electrons, respectively (integrated over final angles for any particular final state or

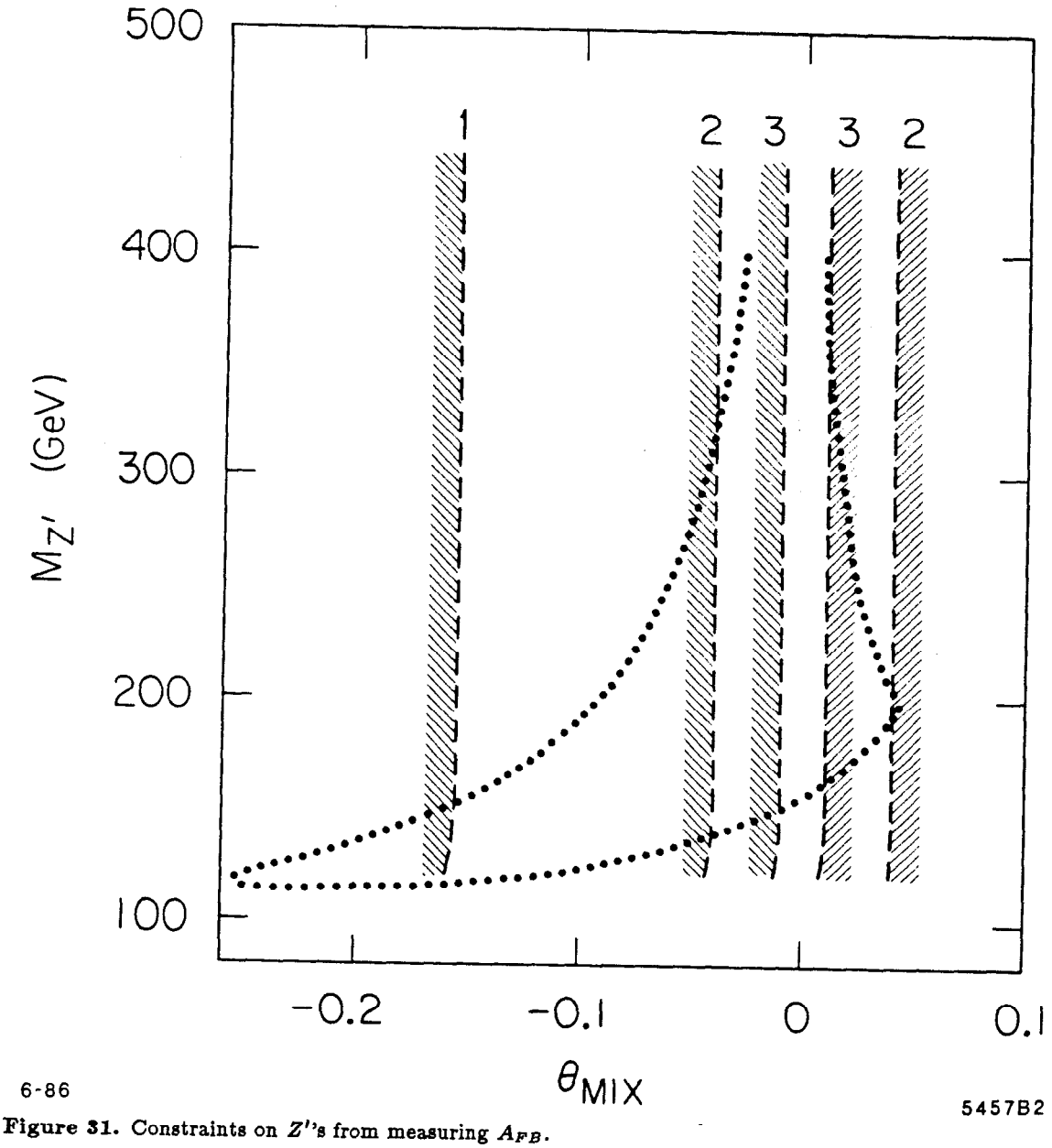

Figure 31. Constraints on Z''s from measuring A_{FB}.

sum of final states), and v_e and a_e are the vector and axial-vector couplings of the Z to electrons. The second equality in Eq. (4.1) is valid only at the peak of the Z. With $\sin^2\theta_W = 0.22$, the polarization asymmetry has a value of about -0.24. More importantly, since v_e happens to be close to zero because of the particular value of $\sin^2\theta_W$ that exists, A_{POL} is very sensitive to deviations from

the standard model; in particular it is sensitive to changes in couplings from small admixtures of a Z' in the Z.[27] Again, these measurements are sensitive to the value of θ_{MIX} and not to that of $M_{Z'}$.

It is possible to consider looking at decays of the Z into particular quark-antiquark channels with a polarized beam. However, it will be very difficult to get the necessary accuracy because of difficulties in identifying a particular quark and the great loss of statistics involved in making the very restrictive cuts on the data necessary to isolate a particular channel.

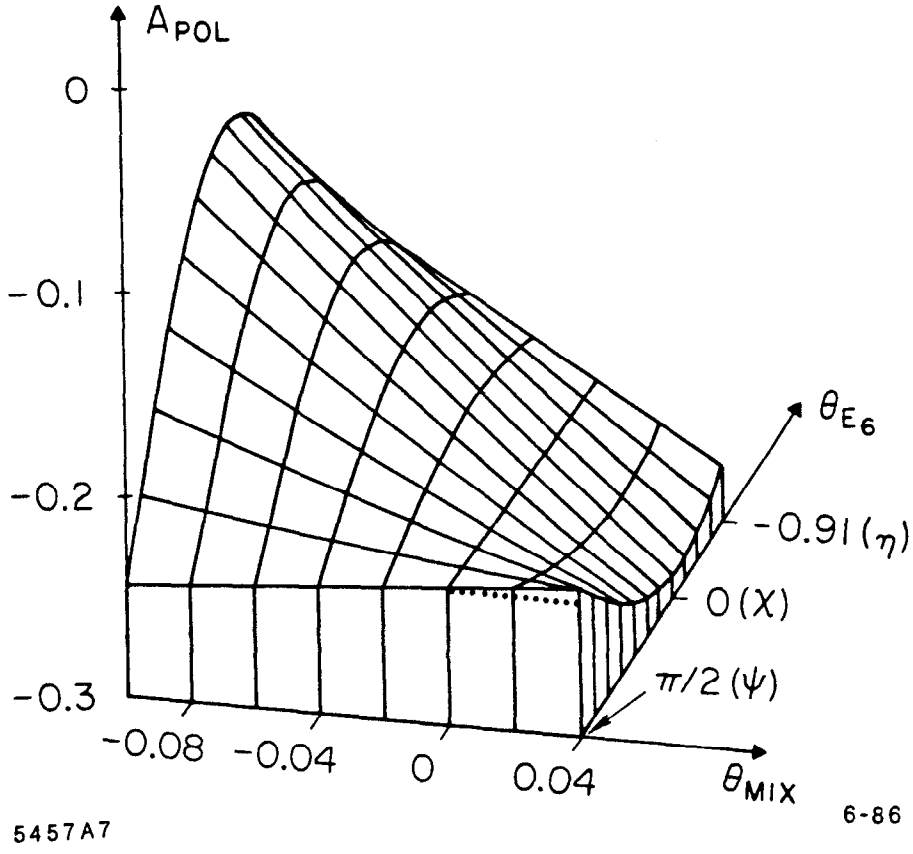

Figure 32. A_{POL} versus θ_{MIX} and θ_{E_6}.

Figure 32 shows A_{POL} at the peak of the Z as a function of both θ_{MIX} and θ_{E_6}. The dotted line is the value of the asymmetry in the standard model with $\sin^2\theta_W = 0.22$ and no Z' present. The effects of mixing are large, particularly for Z_η. They are almost non-existent for Z_ψ, for it has purely axial-vector couplings to electrons and its admixture does not change in lowest order the vector coupling of the Z to electrons (to which A_{POL} is most sensitive).

The corresponding limitations on M_{Z_η} and θ_{MIX} are shown in Figure 33. The boundaries are one sigma limits on the deviation of A_{POL} from the "prediction" of the standard model with no Z'. The dotted curve is the allowed region from Figure 27 for comparison. Even with 10^4 Z's and a 5% systematic uncertainty (solid curve) in the polarization of the beam, the allowed region is as small as can be bounded by the other measurements we have discussed. The dashed curve represents 10^5 Z's and a 3% systematic error. With 10^6 Z's and a 1% systematic uncertainty (dash dot), one will be able to bound $|\theta_{MIX}| \lesssim 0.01$!

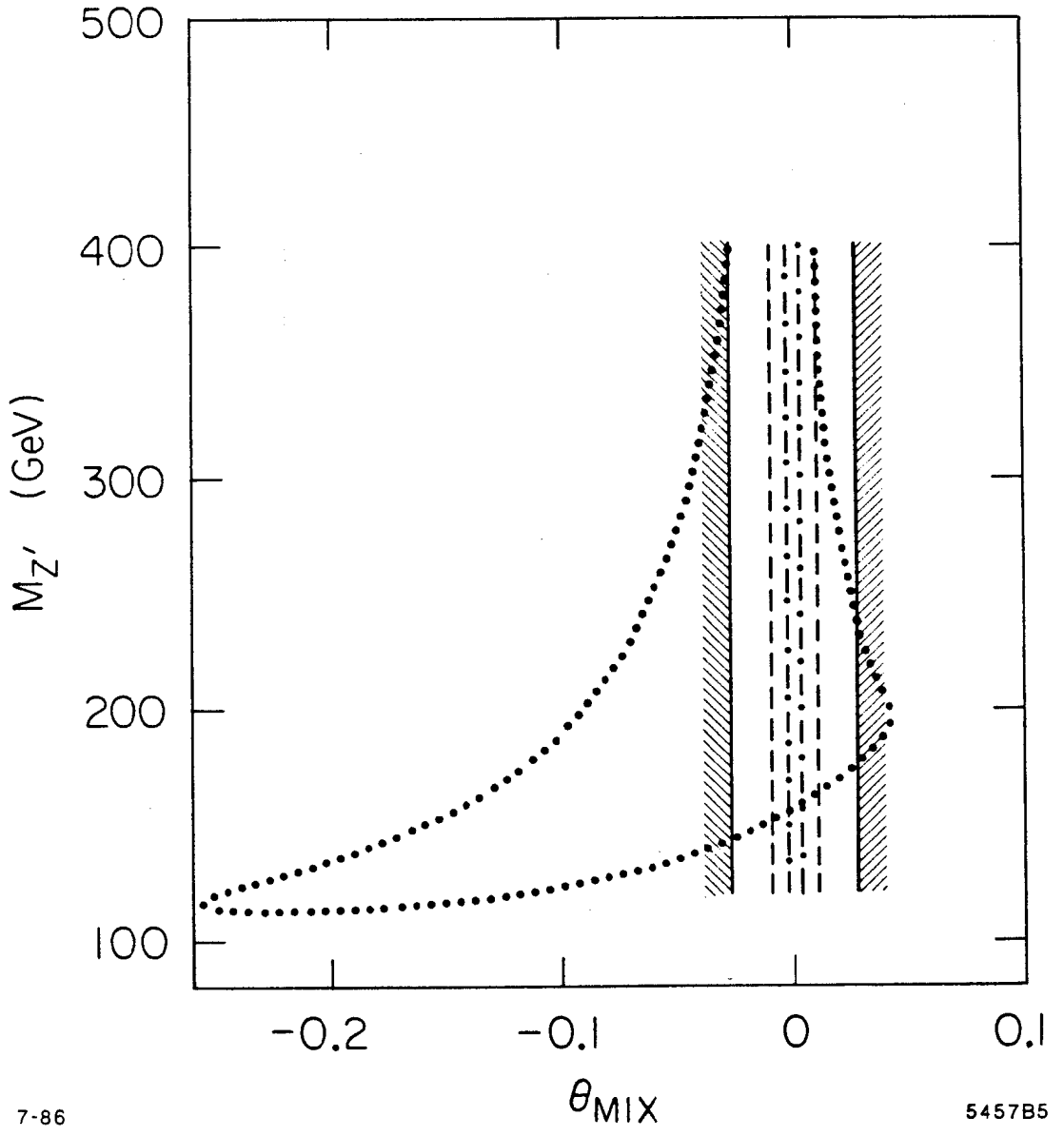

Figure 33. Constraints on Z''s from measuring A_{POL}.

5. Limits from Measurements Above the Z

We have just seen that fairly tight restrictions can be placed on θ_{MIX} from various measurements at the Z peak. However, there is still the possibility that θ_{MIX} is very close to or identically zero. Then the Z is just that of the standard model, and there is no effect worth speaking about at $\sqrt{s} = M_Z$.

But there still are effects off the Z peak, particularly at somewhat higher energies. Even when θ_{MIX} is non-zero it is interesting to look at electron-positron collision energies other than at the Z peak to see the relative sensitivity to a Z'.

Figure 34 shows the front-back and polarization asymmetries as a function of $\sqrt{s}$ for several Z' masses and values of θ_{MIX} and θ_{E_6}. For a Z_η at 150 GeV and $\theta_{MIX} = -0.2$ (solid curve), near the boundary of what is allowed by current experiments (see Figure 27), Figures 34a and 34d show that there are large deviations from what one would expect without a Z' both above and below the Z. Even if $\theta_{MIX} = 0$ (dashed curve) the polarization asymmetry starts to deviate significantly from the standard model at $\sqrt{s} \sim 110$ GeV.

Figures 34b and 34e show that if there is appreciable mixing, there are noticeable deviations in the longitudinal polarization asymmetry starting at $\sqrt{s} \sim 110$ GeV, even if the mass of a Z_η is as high as 300 GeV. The solid curve shows M_{Z_η} = 200 GeV and $\theta_{MIX} = -0.15$ and the dashed curve shows $M_{Z_\eta} = 295$ GeV and $\theta_{MIX} = -0.05$. If $\theta_{MIX} = 0$, there are still 10% changes in A_{POL} 15 GeV above and below the Z. However, the absolute value of A_{POL} and the cross section below the Z are so small that a measurement there will be statistically insignificant. The deviations for the front-back asymmetry are much smaller (less than about

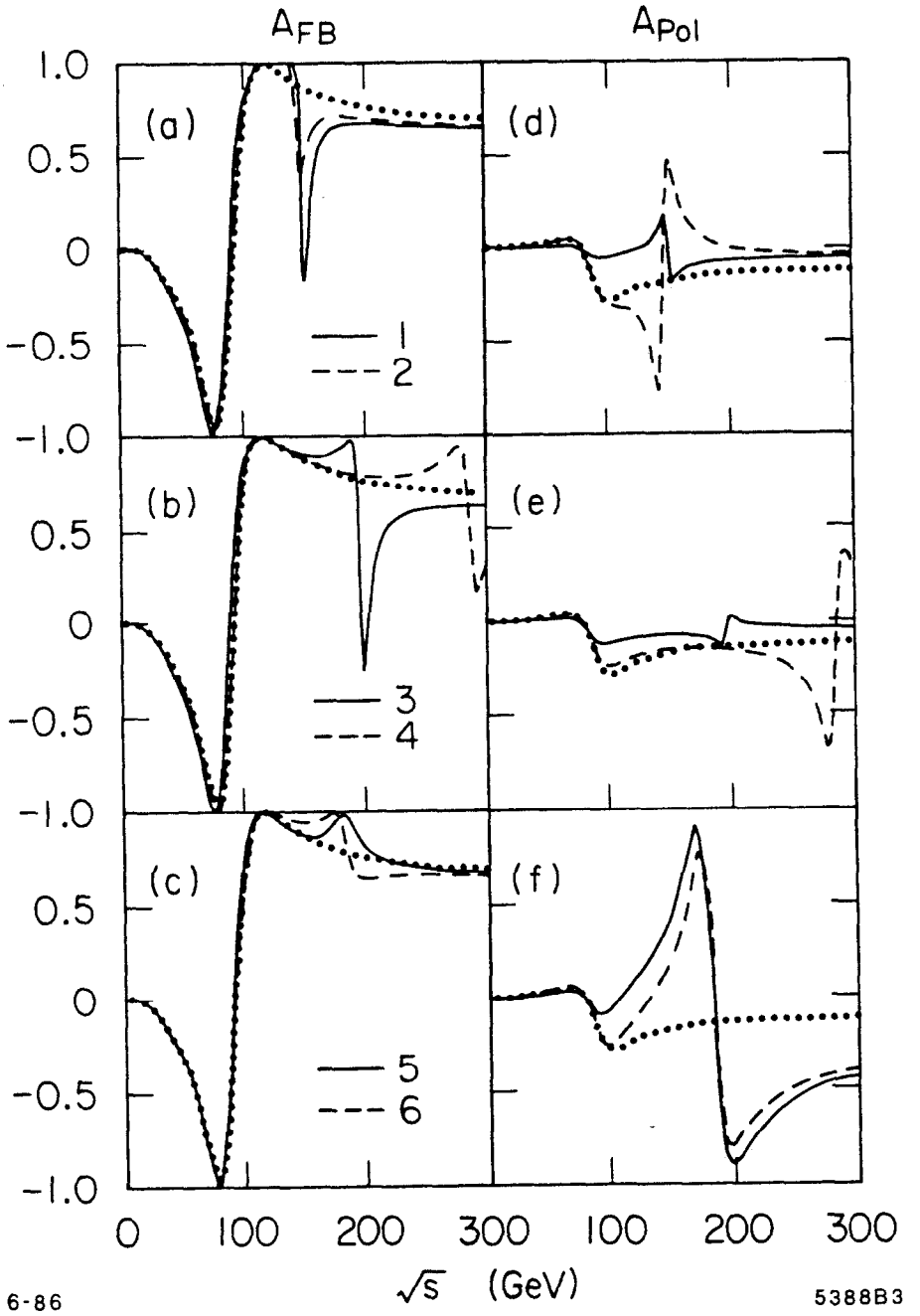

Figure 34. Variations in off-peak asymmetries due to Z'.

1% in this case). Because one must identify a final fermion and distinguish it from the corresponding antifermion, adequate statistical power for a significant measurement of the front-back asymmetry appears to be an insuperable problem away from the Z peak. Figures 34c and 34f show effects in the χ model: M_{Z_χ}= 200 GeV, $\theta_{MIX} = -0.1$ (solid curve), and $\theta_{MIX} = 0$ (dashed curve). The dotted curve is in all the cases the expectation without a Z'.

There are two problems with off-peak effects—the cross section is lower—and hence it will be hard to get running time there. We will quantify the former effect by considering the following expression for the number of σ of the effect off-peak, where the statistical error is scaled according to the produced cross section off-peak.

We have

$$\#\text{ of } \sigma(\sqrt{s}) = \frac{A_{POL}(\sqrt{s})_{\text{with } Z'} - A_{POL}(\sqrt{s})_{\text{s.m.}}}{\Delta A_{POL}} \tag{5.1}$$

where

$$\Delta A_{POL} = \sqrt{\left(\frac{\Delta P}{P} A_{POL}(\sqrt{s})\right)^2 + \frac{5}{N}\frac{187}{R(\sqrt{s})}}. \tag{5.2}$$

The first term comes from the uncertainty ΔP in the polarization of the beam, P. The second term is the statistical error in the actual polarization asymmetry, given by the inverse of the square root of the number of events (the error in the experimentally measured polarization asymmetry), divided by P (taken to be .45). N is the equivalent number of events on the Z peak. Since the total error is statistics dominated, the comparison of off-peak effects to on-peak effects is most favorable when $\Delta P/P$ is large and N is large (and $|\theta|$ is small). The

θ_{mix}	$M_{Z'}$	$\sqrt{s}$	ΔA_{pol}	$\sigma(1\%, 10^6)$	$\sigma(5\%, 10^6)$
$-.01$	200	Z	.009 (.014)	2.9 (4.4)	.8 (1.2)
		100	.004 (.046)	.36 (4.4)	.2 (3.0)
		130	$-.04$ (.133)	-1.4 (6.2)	-1.3 (6.2)
0	200	Z	$-.0001$ (.0001)	$-.04$ (.03)	$-.01$ (.008)
		100	$-.008$ (.036)	$-.7$ (2.7)	$-.4$ (1.8)
		130	$-.05$ (.168)	-1.7 (5.5)	-1.6 (5.5)
0	400	Z	$-.00003$ (.00003)	$-.01$ (.008)	$-.003$ (.002)
		130	$-.008$ (.024)	$-.27$ (.77)	$-.25$ (.74)
		180	$-.019$ (.06)	$-.48$ (1.5)	$-.5$ (1.5)

Table 4. Effects of a Z' on and off the Z peak.

same integrated luminosity that produces 10^6 Z's at the peak will give a ~ 3 σ deviation in the polarization asymmetry (from the standard model value), for $\sqrt{s}$ ~110 GeV, due to the presence of a Z_χ at 200 GeV with $\theta_{MIX} = 0$. Changing the mixing angle to -0.03 yields a $\sim 6\sigma$ effect and it remains near 3 σ for the same mixing angle if, in this favorable case, the mass is raised to 400 or 600 GeV. In Table 4 we show some representative numbers (those in ()'s are effects in the χ model; the others are in the η model) for $\Delta P/P = 1\%$ and 5%, with a luminosity that would produce 10^6 Z's on peak.

In summary, using the extra neutral gauge bosons accompanying the breaking of the grand unification group E_6 down to the standard model as examples, we have seen in this part of the thesis how a Z' could affect electron-positron annihilation experiments. In general the massive physical neutral gauge bosons will be mixtures of the Z of the standard model and the other neutral gauge

bosons. This mixing changes the couplings of the Z from those of the standard model. Accurate measurements of the cross section at the Z peak will provide new constraints on the properties of a Z'. Even more sensitive to these changed couplings is the longitudinal polarization asymmetry; it can be used to limit $\theta_{MIX} \lesssim 0.01$, given anticipated systematic and statistical errors. But even if $\theta_{MIX} = 0$, measurements off the Z peak involving the polarization asymmetry can give decisive evidence for a Z'.

The combination of measurements at the Z and above it is a very powerful indicator of the presence of extra neutral gauge bosons. It should be possible, using these experiments in combination, to rule out (or find evidence for!) the presence of a Z' up to masses several times that of the Z.

REFERENCES

1. M. B. Green and J. H. Schwarz, Phys. Lett. **149B**, 117 (1984) and **151B**, 21 (1985).

2. P. Candelas, G. Horowitz, A. Strominger, and E. Witten, Nucl. Phys. **B258**, 46 (1985); E. Witten, Nucl. Phys. **B258**, 75 (1985).

3. M. Dine, V. Kaplunovsky, M. Mangano, C. Nappi, and N. Seiberg, Nucl. Phys. **B259**, 549 (1985).

4. E. Witten, Nucl. Phys. **B268**, 79 (1986). See also, H. W. Braden, *et al.*, Phys. Rev. Lett. **56**, 2668 (1986).

5. S. M. Barr, Phys. Rev. Lett. **55**, 2778 (1985).

6. J. Ellis *et al*, CERN preprints TH.4323/85 and TH.4350/86, 1986 (unpublished); E. Cohen *et al.*, Phys. Lett. **165B**, 76 (1985).

7. L. S. Durkin and P. Langacker, Phys. Lett. **166B**, 436 (1986).

8. V. Barger, N. G. Deshpande, and K. Whisnant, Phys. Rev. Lett. **56**, 30 (1986).

9. W. Hollik, Z. Phys. **C8**, 149 (1981).

10. P. Wang, Virginia Polytechnic Institute preprint VPI-HEP-85/2, 1985 (unpublished).

11. G. Bélanger and S. Godfrey, TRIUMF preprint TRI-PP-86-12, 1986 (unpublished).

12. V. D. Angelopoulos *et al.*, CERN preprint CERN-TH.4408/86, 1986 (unpublished).

13. M. Cvetič and B. W. Lynn, SLAC preprint SLAC-PUB-3900, 1986, to be published in Phys. Rev. D. M. Cvetič, talk at the Mark II workshop at Asilomar, March, 1986. We thank Cvetič and Lynn for discussions on their work.

14. P. J. Franzini, talk at the XXIth Rencontre de Moriond, March, 1986 and SLAC preprint SLAC-PUB-3920, 1986 (unpublished) gave a preliminary version of this work. See also, F. J. Gilman, invited talk at the 7th Vanderbilt Conference on High Energy Physics, May, 1986 and SLAC preprint SLAC-PUB-4002, 1986 (unpublished).

15. D. Blockus *et al.*, Proposal for Polarization at the SLC, 1986 (unpublished).

16. T. G. Rizzo, Iowa State preprint IS-J-2167, 1986 (unpublished).

17. J. P. Ader, S.Narison, and J. C. Wallet, Montpellier preprint PM : 86-9, 1986 , to be published in Physics Letters.

18. D. Gross, J. Harvey, E. Martinec, and R. Rohm, Phys. Rev. **D54**, 502 (1985).

19. R. N. Cahn, *Semi-Simple Lie Algebras and Their Representations*, (Benjamin/Cummings, Menlo Park, California, 1984).

20. R. Slansky, Phys. Rept. **79**, 1 (1981).

21. P. Langacker, R. W. Robinett, and J. L. Rosner, Phys. Rev. **D30**, 1470 (1984). See also R. W. Robinett and J. L. Rosner, Phys. Rev. **D25**, 3036 (1984) and **D26**, 2396 (1984) and Durkin and Langacker, Ref. 7.

22. See, for example, J. L. Rosner, Comm. Nucl. Part. Phys. **15**, 195 (1986);

P. Binétruy *et al*, Nucl. Phys. **B273**, 501 (1986); D. London and J. L. Rosner, University of Chicago preprint EFI 86-22, 1986 (unpublished).

23. L. DiLella, *Proceedings of the 1985 International Symposium on Lepton and Photon Interactions at High Energies*, Kyoto, Japan, August 19-24, 1985, Eds. M. Konuma and K. Takahashi, p. 280.

24. A similar region was found by V. Barger *et al*, Ref. 8.

25. G. Feldman, private communication.

26. I. Bigi and M. Cvetič, SLAC preprint SLAC-PUB-3966, 1986 (unpublished).

27. The sensitivity of the polarization asymmetry has been noted and analyzed by Bélanger and Godfrey, Ref. 11, Angelopoulos *et al.*, Ref. 12, Cvetič and Lynn, Ref. 13, and Ader *et al.*, Ref. 17.